Tonkie Khimicheskie Tekhnologii = Fine Chemical Technologies. 2023;18(2):135–167

ANALYTICAL METHODS IN CHEMISTRY AND CHEMICAL TECHNOLOGY

АНАЛИТИЧЕСКИЕ МЕТОДЫ В ХИМИИ И ХИМИЧЕСКОЙ ТЕХНОЛОГИИ

ISSN 2686-7575 (Online)
https://doi.org/10.32362/2410-6593-2023-18-2-135-167
UDC 543.5

REVIEW ARTICLE

Analysis of nanoparticles and nanomaterials using X-ray photoelectron spectroscopy

Anatoly A. Ischenko[1,✉], Mikhail A. Lazov[1,✉], Elena V. Mironova[1], Alexey Yu. Putin[1], Andrey M. Ionov[2], Pavel A. Storozhenko[3]

[1]MIREA – Russian Technological University (M.V. Lomonosov Institute of Fine Chemical Technologies), Moscow, 119571 Russia
[2]Institute of Solid State Physics, Russian Academy of Sciences, Chernogolovka, Moscow oblast, 142432 Russia
[3]GNIIKHTEOS, Moscow, 105118 Russia
✉Corresponding author, e-mail: aischenko@yasenevo.ru, lazovm@gmail.com

Abstract

Objectives. *The main aim of this review is to summarize the existing knowledge on the use of X-ray photoelectron spectroscopy (XPS) for the characterization of nanoparticles and nanomaterials.*
Results. *XPS or electron spectroscopy for chemical analysis can provide information on the qualitative and quantitative composition, valence states of the elements of the samples under study, the chemical composition of the surface and interfaces that determine the properties of nanoparticles and nanostructured materials. The review describes the role of several different methods for the characterization of nanomaterials, highlights their advantages and limitations, and the possibilities of an effective combination. The main characteristics of XPS are described. Various examples of its use for the analysis of nanoparticles and nanomaterials are given in conjunction with additional methods to obtain complementary information about the object under study.*
Conclusions. *XPS provides depth information comparable to the size of nanoparticles (up to 10 nm depth from the surface) and does not cause significant damage to the samples. Two disadvantages of XPS analysis are sample preparation requiring a dry solid form without contaminations and data interpretation. XPS provides information not only on the chemical*

identity, but also on the dielectric properties of nanomaterials, recording their charging/ discharging behavior. Chemical information from the surface of nanoparticles analyzed by XPS can be used to estimate the thickness of nanoparticle coatings. XPS has a high selectivity, since the resolution of the method makes it possible to distinguish a characteristic set of lines in the photoelectron spectrum at kinetic energies determined by the photon energy and the corresponding binding energies in elements. The intensity of the lines depends on the concentration of the respective element. Obtaining a sufficiently complete picture of the properties of nanomaterials requires the use of a group of complementary instrumental methods of analysis.

Keywords: *X-ray photoelectron spectroscopy, nanoparticles, nanomaterials, valence states of elements, surface, interfaces, diffraction methods, spectral methods*

For citation: Ischenko A.A., Lazov M.A., Mironova E.V., Putin A.Yu., Ionov A.M., Storozhenko P.A. Analysis of nanoparticles and nanomaterials using X-ray photoelectron spectroscopy. *Tonk. Khim. Tekhnol. = Fine Chem. Technol.* 2023;18(2):135–167 (Russ., Eng.). https://doi.org/10.32362/2410-6593-2023-18-2-135-167

ОБЗОРНАЯ СТАТЬЯ

Анализ наночастиц и наноматериалов методом рентгеновской фотоэлектронной спектроскопии

А.А. Ищенко[1,✉], М.А. Лазов[1,✉], Е.В. Миронова[1], А.Ю. Путин[1], А.М. Ионов[2], П.А. Стороженко[3]

[1]*МИРЭА – Российский технологический университет (Институт тонких химических технологий им. М.В. Ломоносова), Москва, 119571 Россия*
[2]*Институт физики твердого тела Российской академии наук, Черноголовка, Московская область, 142432 Россия*
[3]*Государственный научный центр Российской Федерации АО “ГНИИХТЭОС”, Москва, 105118 Россия*
✉*Автор для переписки, e-mail: aischenko@yasenevo.ru, lazovm@gmail.com*

Аннотация

Цели. *Основная цель данного обзора – обобщить существующие знания об использовании метода рентгеновской фотоэлектронной спектроскопии (РФЭС) для характеризации наночастиц и наноматериалов.*
Результаты. *Метод РФЭС или электронной спектроскопии для химического анализа может предоставить информацию о качественном и количественном составе, валентных состояниях элементов исследуемых образцов, химическом составе поверхности и границ раздела, которые определяют свойства наночастиц и наноструктурных материалов. В обзоре описана роль нескольких различных методов для характеристики наноразмерных материалов, подчеркнуты их преимущества, ограничения и возможности эффективной комбинации. Описаны основные характеристики РФЭС. Приведены различные примеры ее использования для анализа наночастиц и наноматериалов в совокупности с дополнительными методами для получения комплементарной информации об изучаемом объекте.*

Выводы. *РФЭС предоставляет информацию о глубине, сравнимой с размером наночастиц (до 10 нм глубины от поверхности), и не вызывает значительного повреждения образцов. Двумя недостатками анализа РФЭС являются подготовка образцов (требуется сухая твердая форма без загрязнения) и интерпретация данных. РФЭС предоставляет информацию не только о химической идентичности, но и о диэлектрических свойствах наноматериалов, регистрируя их поведение при зарядке/разрядке. Химическая информация с поверхности наночастиц, проанализированная с помощью РФЭС, может использоваться для оценки толщины покрытий наночастиц. РФЭС обладает высокой селективностью, поскольку разрешающая способность метода позволяет различить характерный набор линий в фотоэлектронном спектре при кинетических энергиях, определяемых энергией фотонов и соответствующими энергиями связи в элементах. Интенсивность линий зависит от концентрации соответствующего элемента. Получение достаточно полной картины свойств наноматериалов требует использования группы взаимодополняющих инструментальных методов анализа.*

Ключевые слова: *рентгеновская фотоэлектронная спектроскопия, наночастицы, наноматериалы, валентные состояния элементов, поверхность, границы раздела, дифракционные методы, спектральные методы*

Для цитирования: Ищенко А.А., Лазов М.А., Миронова Е.В., Путин А.Ю., Ионов А.М., Стороженко П.А. Анализ наночастиц и наноматериалов методом рентгеновской фотоэлектронной спектроскопии. *Тонкие химические технологии*. 2023;18(2):135–167. https://doi.org/10.32362/2410-6593-2023-18-2-135-167

INTRODUCTION

As a rapidly growing class of materials, nanostructures are of great interest for many applications. Several methods are used to characterize the size, crystal structure, elemental composition, and many other physicochemical, chemical, and physical properties of nanoparticles. The different strengths and weaknesses of each method make it difficult to choose the most appropriate one, and a combined approach to characterization is often required. In addition, it is necessary that researchers from different fields overcome the problems of reproducibility and reliable characterization of nanomaterials after their synthesis and further processing (e.g. annealing steps).

Determination of the structure, qualitative and quantitative chemical composition of nanomaterials consisting of nanoparticles (quantum dots) or nanofilms (two-dimensional structures), and the relationship of these characteristics with spectral properties is one of the central problems in the study of nano-objects.

The method of X-ray photoelectron spectroscopy (XPS) or electron spectroscopy for chemical analysis, as shown in the proposed review, can provide information on the qualitative and quantitative composition, valence states of the elements of the samples under study, the chemical composition of the surface and interfaces that determine the properties of nanostructured materials.

The number of studies using XPS has increased more than 15-fold over the past 30 years. In the last year alone, XPS has been mentioned in more than 9000 published articles.

XPS is not usually considered as a method with horizontal (lateral) nano-resolution. However, the electrons detected by this method travel distances measured in nanometers and can be used to obtain sufficient information about the structure of nanometer-sized samples on the surface and in the near-surface layer. Although the possibility of obtaining information at the nanometer scale from samples with a flat surface seems more obvious, XPS data can be used to determine the composition of nanoparticles. It is also possible to obtain information about coatings and layers in nanoparticles under conditions where other surface investigation methods cannot be applied.

The main purpose of the review is to summarize the existing knowledge on the use of the XPS method for the characterization of nanoparticles and nanomaterials.

NANOMATERIALS

Nanomaterials are materials that have linear dimensions in one or more directions from a few nm to 100 nm (Fig. 1). Restrictions on the size of nanostructures make it possible to divide them into zero-, one-, two-, and three-dimensional [1–3].

Nanomaterials occupy an intermediate position between atoms and bulk crystalline and amorphous solids. In this regard, the unique properties of nanoparticles are determined by surface (high ratio of the fraction of surface atoms to volume) and quantum-size effects, especially when the particle sizes are comparable with the correlation radii of physical phenomena (the mean free path of electrons, phonons, the size of the magnetic domain or exciton, etc.). The electronic properties of the material depend on these factors, from which many physical and physicochemical characteristics follow, for example, the presence of unique optical, electrical, magnetic, mechanical, catalytic properties, as well as the possibility of surface functionalization [2, 3]. Features of the electronic properties, which manifest themselves as the particle size approaches nanometers, are described in monograph [3] and a number of review articles (see, for example, [4–7]). Quantum size effects of semiconductor nanoparticles are described in textbooks [8–10]. The size effects are also considered in articles [11, 12], the description of the influence of the size of nano-objects on their various properties is given in [13].

In addition to size, in some cases, the shape (magnetic nanocrystals) also has a great influence on the properties of particles [2]. Catalytic activity and selectivity, electrical and optical properties, and melting temperature are also highly shape dependent [14].

Metals that do not exhibit or weakly exhibit catalytic activity in the ordinary state may turn out to be active catalysts in the nanoscale state. The increase in activity is explained by charge transfer from the substrate and is more pronounced for particles with the smallest size [15–19] and those consisting of transition metal oxides [20–24]. Zeolites are often used as a matrix for stabilizing metal nanoparticles, since the particle size can be limited by the channel width [25–31].

In [32], copper oxides (Cu_2O, CuO) were deposited on the surface of SiO_2 and ZrO_2 substrates. It was shown that the values of the binding energy and the modified Auger parameter [33] for copper oxide strongly depend on the degree of dispersion of the deposited phase and the type of substrate.

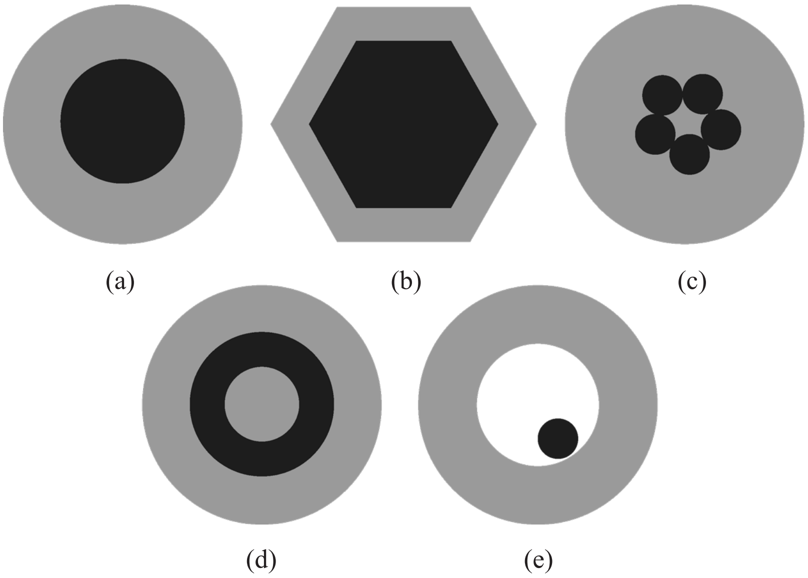

Fig. 1. Nanoparticles with a core–shell structure of various shapes: (a) spherical concentric, (b) hexagonal (hexahedral), (c) nanoparticles containing several cores covered with one shell, (d) multilayer concentric spherical nanoparticles (*nanomatryoshka*), (e) particles with a removable layer [2].

Thus, from the Wagner plots [33], it is possible to determine not only the chemical state of the metal in the deposited layer, but also the particle size distribution [34] (Fig. 2).

One of the modern methods for obtaining nanostructures in the form of thin oxide films under ultrahigh vacuum conditions followed by in situ analysis is the reduction of the surface of higher metal oxides by bombardment with inert gas ions (He^+, Ne^+, Ar^+) or the oxidation of the metal surface with O_2^+ ions. This technique was used to modify and study pressed powdered higher oxides of molybdenum and tungsten [35], tungsten oxide [36], the surface of metallic vanadium [37], niobium oxide [38], and tantalum oxide [39, 40].

A review article [2] is devoted to core–shell nanoparticles, according to which these nanoparticles are used in biomedical and pharmaceutical applications, catalysis, electronics, and are used to achieve a high quantum yield and create photonic crystals (Fig. 3). Applications are also described in [41–43]. Supramolecular systems in general, including nanoparticles, nanomaterials, and structures based on them, are described in [44].

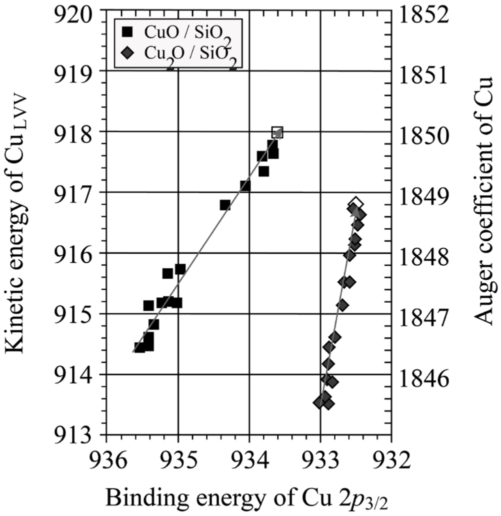

Fig. 2. Wagner plots describing the change in binding energies, kinetic energies, and modified Auger parameters for Cu $2p_{3/2}$ and Cu L_1VV copper lines. The arrow shows the increase in particle size; empty squares correspond to bulk oxides [34].

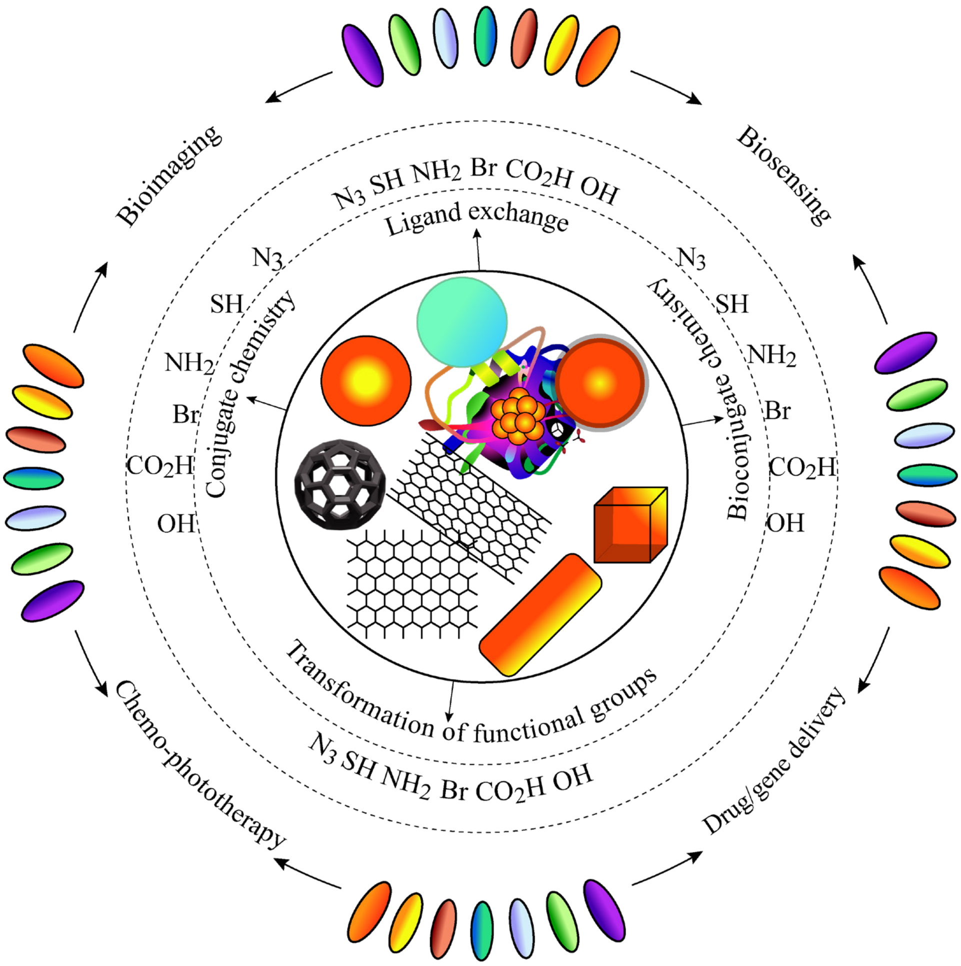

Fig. 3. Fields of application of core–shell nanoparticles [2].

Study of nanomaterial properties

Work [45] is devoted to the commercialization of nanobiotechnologies. Many of the physical and chemical parameters needed to understand the properties of objects are often unpublished and most likely not defined at all. Bureau International des Poids et Mesures, Consultative Committee for Amount of Substance: Metrology in Chemistry and Biology, and Technical Committee of the International Organization for Standardization (TC ISO 229) determined the requirements for nanomaterials in relation to the environment, health and safety, toxicology, and also approved a list of necessary physicochemical properties and parameters of nanomaterials (16 in total) related to the chemical and physical state of the surface [46].

Review [47] is devoted to the methods of studying nanoparticles and nanomaterials. Review [48] summarizes research tools and methods for studying the surface of solids and surface layers developed over the past 50 years. Publication [49] describes the determination of nanomaterials in the environment by various methods.

The papers [11, 48, 50] describe the necessary requirements for the correct analysis of nanoparticles:

1) *in situ* analysis or immediately after synthesis;

2) understanding the interactions (and time dependence) of particles placed in a working environment (biological, solutions, catalysis, etc.);

3) the need for analysis by several methods;

4) development of new methods of analysis, or increasing the resolution and sensitivity of already used methods to obtain more accurate information about the structure of nanomaterials.

Since nanomaterials, like colloidal systems, are qualitatively different from the bulk substance, it can be assumed that methods previously developed for colloidal systems can be used to analyze nanomaterials. However, despite the similarity of these objects, colloidal phenomena can lead to the degradation of nanomaterials [51].

Ultra-microscopy using visible light can determine the limiting particle size of the order of 200 nm (taking into account the boundaries of the visible range of 400–700 nm), and using ultraviolet—up to 100 nm. When light scattering is used, the limiting determinable size of nanoparticles is 2–5 nm, which is an adequate approach for nanoparticle sols. The limitation of this method is the need to measure dilute sols and a significant difference between the refractive index of the dispersed phase (nanoparticles) and the dispersion medium [52]. Other methods based on the scattering of light by particles are nephelometry and turbidimetry, suitable for estimating particle sizes in dilute sols. To determine the particle size distribution, ultracentrifugation and the construction of sedimentation curves are used. To determine the surface potential of charged particles (ζ potential), measurements of electrophoretic braking and electro-osmosis are carried out [52].

The method of X-ray diffraction with a particle size of less than 5 nm becomes severely limited in terms of analytical information, there is no surface sensitivity, and a sufficiently large amount of substance and time are required for analysis. Electron microscopy, X-ray diffraction, and electron diffraction are more versatile and have a resolution sufficient for studying nanomaterials [3].

The Mössbauer spectroscopy method provides information on the short-range order of the structure of matter and magnetic properties at different temperatures and external magnetic fields [52].

Transmission electron microscopy (TEM), atomic force microscopy (AFM), Brunauer–Emmett–Teller (BET) specific surface area measurements provide information on size and size distribution, particle shape, and surface properties. TEM can also determine the crystallinity of a sample. AFM determines the height distribution, location, and size of particles. If this information is lacking, the BET method is used, provided that the particles have a narrow size distribution, are spherical in shape and are not porous. An estimate of the external size (hydrodynamic diameter) of a particle of regular shape can be determined by the method of dynamic light scattering [3, 52].

Scanning electron microscopy (SEM) is used to determine the structure and size distribution of particles, but is inefficient for measuring samples consisting of complex nanoparticles (for example, with a core–shell structure), since it provides information only about the size distribution for the whole particle. Under the action of an electron beam, the surface structure changes. SEM gives inadequate results when determining the particle size less than 20 nm. The method of electron diffraction on a selected region has limitations associated with measuring the signal from a large number of crystalline particles (to determine crystallinity) and a sufficiently large fraction of amorphous nanoparticles in a crystalline matrix for their detection [52].

Electrophoretic light scattering (laser Doppler electrophoresis) is used to determine the charge on the particle surface.

Infrared spectroscopy and paramagnetic resonance spectroscopy determine the presence of adsorbed light molecules and functional groups on the surface of particles and the degree of substitution of surface atoms. When measuring absorption and luminescence spectra in the optical region, one can determine the surface roughness, film thickness, and particle size due to the difference in the properties of nanomaterials from bulk materials [3, 52].

Thermal analysis (thermogravimetry), differential thermal analysis and differential scanning calorimetry allow you to study phase transitions in a substance, including glass transition and crystallization into various polymorphic phases. Using these methods, the characteristics (temperature, energy) of the above processes and the phase composition of the resulting nanoparticles are determined. When carrying out isothermal calorimetric titration, it is possible to determine the ability of sorption of proteins and biologically active substances [52].

There are also other methods such as vibrational and superconducting quantum interference device magnetometry (superconducting quantum interferometer is a supersensitive magnetometer used to measure very weak magnetic fields), energy dispersive and X-ray absorption spectroscopy, electron energy loss spectroscopy, X-ray spectroscopy of absorption near the edge and with high resolution (fine structure) [3, 52]. Works [53–56] are devoted to modern methods of studying nanoparticles and nanomaterials, up to the determination of the structural dynamics of individual molecules in the femtosecond range.

XPS is one of the most reliable methods for determining the electronic structure and stoichiometry of solids. General information about measurements of samples by this method is given, for example, in [57]. Some deviations of the results may occur due to adsorbates present on the surface of the studied particles [58].

General conclusions about the analysis of nanoparticles

Some of the main unresolved issues in the field of nanoparticle research are the following [52, 59]:

1) the instability of nanomaterials and nanoparticles, which significantly increases the requirements for the influence of the analysis tool, external conditions, measurement conditions and time on the materials under study;

2) a significant proportion of atoms or molecules and the possible influence of surface impurities, elemental enrichment or depletion and contamination;

3) the need to use complementary methods to increase the significance (correctness) of the information received;

4) change in the physical properties of nanomaterials, for example, the mean free path of electrons or the etching rate of surface atoms by ions, associated with size and environment;

5) increased requirements for sample preparation for analysis.

XPS OF NANO-OBJECTS

With the development of nanotechnologies, the role of XPS as a surface analysis method has increased significantly. A feature of this method is the possibility of qualitative and quantitative chemical analysis of the surface layers of a substance—multiphase and multicomponent thin films, particles, and powders on the surface. It is possible to analyze the fine structure of the spectra and determine the charge and chemical states of the detected elements. Determination of the qualitative and quantitative composition is acceptable in depth (profiling) and on the surface (mapping).

The lateral resolution of electron spectrometers is usually a few micrometers and exceeds the size of typical nanoparticles by at least three orders of magnitude, so the area of information collection is determined by the shallow depth of analysis based on the mean free path of photoelectrons. The analytical depth is 4–10 nm for polymers, and 0.5–2.5 nm for metals and oxides. Another advantage is that XPS is a non-destructive analysis method, which allows signal accumulation from low-intensity components. The exception is polymeric and photosensitive samples, for which slight photodissociation and radiolysis are possible. The lower limit of the determined concentrations is ~0.1 at. %, which corresponds to 1–10 ng of a substance or 0.01–0.05 of a monolayer.

General provisions

XPS measurements are usually carried out under ultrahigh vacuum conditions to prevent adsorption of molecules and contamination of the surface during the measurement process. Recently, near-atmospheric pressure systems (near-ambient pressure XPS) have also been developed and used, both with synchrotron sources and conventional X-ray tubes [60, 61].

Under conditions of ultrahigh vacuum, it is possible to analyze impurities and surface defects, and at elevated pressure, it is possible to study reactions on the surface, in particular, catalysis. Many photoelectron spectrometers are combined with *in situ* sample preparation tools such as molecular beam epitaxy, pulsed laser deposition, chemical vapor deposition, magnetron sputtering, and ion bombardment. The XPS method in relation to the study of classical objects, for example, the surface of solids, is described in detail in a number of textbooks and monographs [62–67].

Structure of the device

The main components of a modern electron XPS spectrometer (Fig. 4) are a radiation source, a device for mounting and introducing a sample, an energy analyzer, and an electron detector located in an ultrahigh vacuum chamber [68–71].

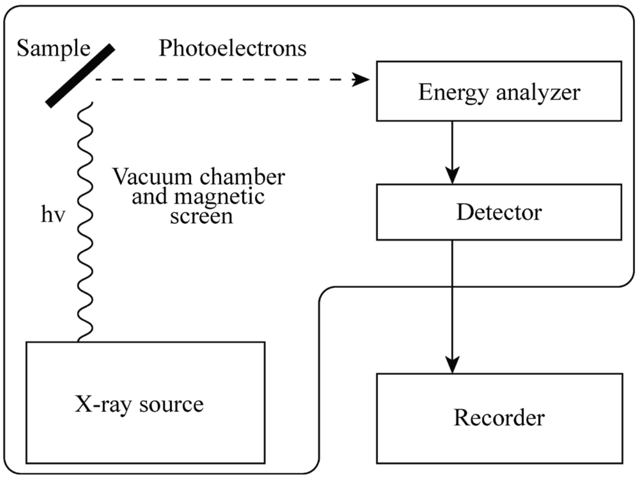

Fig. 4. Block diagram of an X-ray photoelectron spectrometer.

The radiation sources in the XPS method, as a rule, are X-ray tubes with a metal anode, which give soft characteristic X-ray radiation with an energy of the order of several keV, which makes it possible to carry out a qualitative and quantitative elemental analysis of the sample surface, determine the chemical state (oxidation state) of elements, and also investigate the electronic the structure of valence states near the Fermi level (with a rather low resolution of the spectra) [70, 72–74]. The energy resolution of the XPS method is determined primarily by the bandwidth of the exciting radiation. The resolution can be increased using monochromators, which also leads to some side effects [75–79].

XPS is a method of integral analysis due to the rather large diameter of the X-ray beam. Local analysis is possible when the spectrometer is equipped with sharp-focus X-ray tubes with a beam diameter of 100–500 μm.

As a detector in XPS, a secondary electron multiplier is used, which is a proportional electron counter and amplifies the signal by a factor of 10^6–10^7. Industrial spectrometers use channel electron multipliers or large area detectors or vidicon detectors [69, 70, 72].

To ensure a sufficient mean free path of electrons without energy dissipation and loss of analytical information, as well as to maintain surface cleanliness, ultrahigh vacuum with a pressure of 10^{-6}–10^{-8} Pa is maintained in the spectrometer during measurements, supported by various types of pumps. The requirement for surface cleanliness imposes a limitation on the materials used in the spectrometer device.

There are a number of methods developed from classical XPS. These are valence band XPS (using gas-discharge sources), energy loss spectroscopy (on such features of the electronic structure of the sample as surface and bulk plasmons, shake-up satellites, asymmetric core lines, and multiplet splitting), photoelectron diffraction. Modification of the spectrometer design led to the appearance of photoelectron spectroscopy with angular resolution and the introduction of synchrotron and ultraviolet radiation sources [62, 68, 70, 72].

Method basics

Spectra measurement. When analyzing a sample, the survey spectrum is first measured over a wide range of binding energies. The survey spectrum consists of photoelectron and Auger lines, satellites from an X-ray source and shaking and contains a background of inelastically scattered electrons. Following that, the boundaries of photoelectron lines are determined and the spectra of individual lines are measured [70, 71] (Fig. 5).

Mathematical processing of the spectra is described in detail in the sources [80–82]. There are also some additional data tables that allow one to manually or programmatically subtract the spectrum features (X-ray satellites) associated with the non-monochromaticity of the source [75, 83].

Determining the chemical state of atoms on the surface is possible by changing the binding energy of the line with a change in the environment of the atom (chemical shift). There are a large number of works on theoretical calculations of the chemical shift and absolute binding energy, however, in practice, insufficiently accurate knowledge of the numerical parameters required for calculations leads to the need to refer the obtained experimental data to the data measured for standard samples. The rules for determining

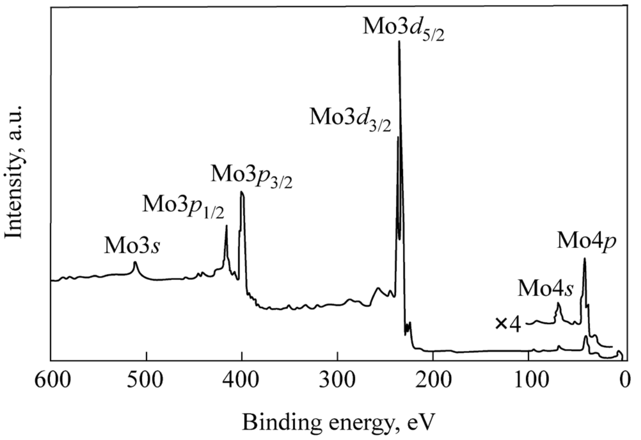

Fig. 5. X-ray photoelectron spectrum of molybdenum upon excitation by Mg Kα radiation, recorded at an analyzer transmission energy of 100 eV [70, 71].

the chemical shift indicate that the chemical shift of the element line depends on the oxidation state of the element in the compound under study, which is equivalent to the electron density distribution between the atom and adjacent atoms, or the charge on the atom [70, 83]. Under conditions of electrostatic charging, which occurs when measuring poorly conducting or dielectric samples, the spectra are completely shifted to the region of high binding energies. In some cases, this effect can be minimized by irradiating the sample surface with a compensating low-energy electron beam. In other cases, for the qualitative determination of elements or chemical states, either assignment to lines with a reference binding energy (for example, Ag 3*d*, Au 4*f*, or C 1*s*) is used, which may not be true with differential charging, or the determination of the qualitative composition and forms of the substance by the usual or modified Auger parameters [83].

Quantitative analysis in XPS

Classical quantitative analysis via photoelectron spectra is based on the fact that line intensities are directly proportional to element concentrations and elemental sensitivity factors [68–70]. Most of the parameters of the photoemission process significantly depend on the material, their ratio is close to a constant value, so the fraction of atoms of a given type C_x in the sample can be determined by Eq. (1):

$$C_x = \frac{I_x / S_x}{\sum_i I_i / S_i}, \qquad (1)$$

where I_x is the line intensity, S_x is the elemental sensitivity factor. A set of elemental sensitivity factors is required for each X-ray source with a different angle between the source and the energy analyzer. The sensitivity factors for a homogeneous sample are determined as the product of the photoionization cross section of the atomic shell σ_i and the mean free path for photoelectrons of a given line λ_i [83].

A table of theoretically calculated photoionization cross sections for atomic orbitals (from lithium to uranium) was given in the reference book[1]. The National Institute of Standards and Metrology (NIST) maintains six databases applicable to XPS and Auger spectroscopy. These are databases on the binding energies of photoelectronic lines in XPS, on the elastic scattering cross sections of electrons, on the mean free paths of electrons in a substance, on the effective electron (in)elastic mean free paths in a substance, on modeling electronic spectra for surface analysis, and on backscattering correction factors for Auger-spectroscopy.Critical reviews [84–87] are devoted to the evaluation of these data.

When determining atomic concentrations, the following assumptions are usually made:

1) in the area of analysis, the sample is homogeneous or polycrystalline (up to the information depth of measurement over the entire analyzed area);

2) reflection and refraction of X-rays is negligible;

3) reflection and inelastic scattering of photoelectrons is small;

4) the probability of photoionization of core levels does not depend on the environment of atoms (low matrix effect);

5) the area of the X-ray beam exceeds the area of the sample.

Changes in the elemental sensitivity factors of transition metals in different compounds can be taken into account using the experimental values measured for different standard samples [83].

When the composition of the sample is inhomogeneous, calculations by Eq. (1) lead to errors. These deviations can be eliminated by taking into account additional factors affecting the peak intensities [70–73]:

1) measurement of elemental and complex, close in composition, standard samples under the same conditions as a sample of unknown composition;

2) introduction of corrections for the depth of exit and the atomic density changed in comparison with the standard (matrix correction);

---

[1] https://xpslibrary.com/%CF%83-sf-asf-and-rsf/. Accessed April 01, 2023.

3) modeling the spectra obtained for the assumed concentration gradients, if they are well known, and performing a multicomponent fitting, taking into account the resulting background of inelastically scattered electrons.

Ultraviolet photoelectron spectroscopy (UPS)

According to the principle of operation, UPS is similar to XPS [73, 75, 83, 88]. As radiation sources, gas-discharge lamps are used, which, depending on the pressure of the inert gas, emit lines of He I (21.2 eV) and He II (40.8 eV) or Ne I (16.9 eV) and Ne II (26.8 eV) with a very small linewidth (less than 0.02 eV). In lamps, a capillary discharge with a cold cathode occurs [88].

UPS is not a method for quantitative surface analysis, since it does not give a quantitative estimate of the atomic concentrations of elements on the surface. The lines in the region of the valence band have a large width (3–5 eV), and the intensity depends on the bonds formed by the element and differs for a number of compounds. Therefore, the shape of the valence band spectra differs for isomers and allotropic modifications, which is used to distinguish between surface compounds, for example, amorphous carbon, graphite, and highly oriented porous carbon [88].

This method makes it possible to record the spectra of states of valence electrons near the Fermi level and quasi-core levels with a low binding energy with a high energy resolution and intensity. UPS in the variant with angular resolution was intensively used in studies of the binding energy of adsorbates with the surface, and when measuring the photoelectron spectra of a smooth surface of single-crystal samples at different polar and azimuthal angles, it is possible to construct a band structure [88].

XPS with synchrotron excitation

The use of synchrotron radiation sources for excitation of photoemission offers advantages over X-ray tubes commonly used in laboratory instruments. Synchrotron XPS measurements can be more efficient due to the unique characteristics of synchrotron radiation compared to X-rays, especially with respect to nanomaterials [89]. The most important advantages are high intensity and brightness, the possibility of tuning the radiation energy, high energy resolution, and low linewidth after the monochromator (depends on the radiation energy, is less than 0.1 eV for energies of the order of keV).

The concept of brightness includes illumination and angular divergence of the beam. Due to the fact that synchrotron sources have a brightness 10^9 times higher than laboratory sources and a small beam size, they are able to provide higher lateral resolution and signal-to-noise ratio. This can be especially significant when measuring spatially separated nanoparticles at low surface coverage [89].

The high energy resolution of modern electron analyzers, ultraviolet and synchrotron radiation, high angular resolution (fractions of a degree), and ultralow temperatures have made it possible to make significant progress in experimental studies of the electronic structure of the valence bands of solids. As a result of such experiments, experimental Brillouin zones, Fermi surfaces, and zone dispersion maps are obtained, which previously could only be obtained from quantum chemical calculations.

The width of the photoelectron peaks is determined by the convolution of three components: the natural linewidth, the resolution of the electronic analyzer of the spectrometer, and the width of the exciting radiation. The natural width of the lines depends on the atomic orbital from which the photoemission occurs and is usually in the range of 0.13–0.70 eV (for Ag $3d_{5/2}$ it is 0.33 eV). In instruments with synchrotron sources and X-ray tubes, approximately the same electron analyzers are used, and the difference in resolution is due to the width of the X-ray line. The linewidth of synchrotron radiation is a function of the radiation energy and monochromatization and is much lower than that of X-ray tubes. This makes it possible to track small (smaller) chemical shifts [90].

Currently, there are new methods of XPS with synchrotron radiation or free electron lasers at high pressure. One of the promising and fairly new areas is the study of heterogeneous processes at the solid–liquid interface, which includes the preparation of thin liquid films and XPS measurements at high (atmospheric) pressure (Fig. 6) [91–93]. Chemical shift measurements can provide high chemical selectivity for both molecules on the surface and the substrate. In XPS experiments with X-ray quanta with an energy of ~1 keV, it is possible to create pressures in the range of several Torr and even higher due to the generation of photoelectrons with a high kinetic energy and a long mean free path [91].

In [93], the interface between metallic nickel and an aqueous solution of KOH was studied using synchrotron radiation sources, differential pumping systems between the sample and an electron analyzer.

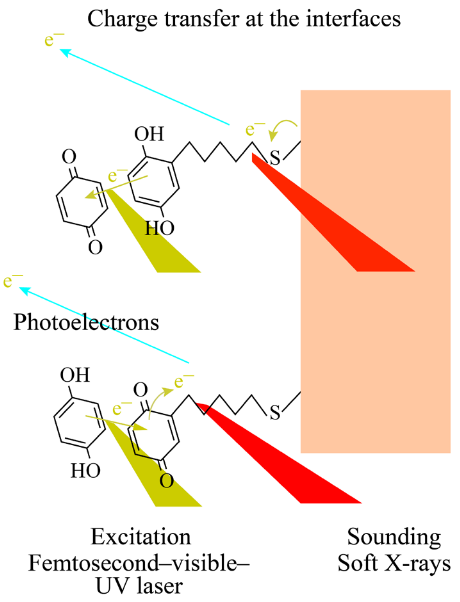

Fig. 6. Investigation of heterogeneous processes at the solid–liquid interface using XPS [91].

Excitation was carried out by radiation converted into a standing wave, which was achieved by using a multilayer Si/Mo mirror as a substrate and increased the depth resolution [93]. Previously, the same team of researchers carried out work to determine the surface layer of α-hematite (Fe_2O_3) adjoining a solution containing high concentrations of NaOH and CsOH [91]. The measurements were carried out at elevated pressure, using a multilayer substrate that provides the formation of a standing wave (ambient pressure XPS (AP XPS); standing wave ambient pressure photoelectron spectroscopy). Using XPS with angular resolution, it was determined that when moving away from the surface of hematite as a solid, there is a mixed hydrated layer with adsorbed NaOH, then a layer of NaOH and CsOH adsorbate, and then a layer of hydrocarbon contamination. Thus, the experimental data are consistent with the theoretical models. As another example of the use of the AP XPS method, one can cite the work [94], where core–shell nanoparticles consisting of strontium/calcium fluoride in ethylene glycol were studied.

Freezing is used to measure biological samples or thin liquid films on a surface in addition to measurements at elevated pressure. The study of electrocatalysts for fuel cells using XPS is described in review [95]. From the simulation of water adsorption on the Pt (111) surface, it followed that a thin ice film is bound to the metal surface by metal–oxygen and metal–hydroxyl bonds. Also in the review, the structure of iodine adsorbate on the surface of a gold single crystal was studied with a change in the voltage between the surface and the solution, which is of interest from the point of view of the oxidation/reduction potential of the iodide–ion/iodine pair associated with oxidative desorption and reductive deposition on the surface. Similar results were obtained for Pt (111) and Pt (111) surfaces with 0.5 Ru, Ru (0001) monolayers.

In the same work, a linear correlation was found between the adsorbate chemical shift and the adsorption energy of ultrathin metal films and molecules. Further, for real fuel cells consisting of platinum on a carbon carrier, the relationship between the oxidation state and the chemical shift and the spin–orbit splitting, which are different for oxide and metallic platinum, was determined. For catalyst particles consisting of an alloy of various metals (Pt/Ni, Pt/Ru, Pt/Ru/Ni), the dependence of the binding energy of platinum lines and the rate of methanol oxidation were determined. Other metals were present in the particles in the oxidized form ($Ni(OH)_2$ and $Ru/RuO_2/RuO_3$) and acted as oxygen donors in this process [95].

It was shown in [96] that the binding energy of the surface of an oxide nanoparticle in solution is related to the surface potential. This result was obtained by measuring a microjet containing silicon oxide nanoparticles. On the surface of oxides, due to interaction with hydroxyl groups in aqueous solutions, a charge is formed, which depends on the composition of the oxide, pH of the solution, its composition, concentration of components, particle size, and the electric field determines many physical and chemical properties of the particles.

The acidity and basicity of the surface groups can be determined from the change in the binding energy of the element. In [97], the polymers were sorted by increasing Lewis basicity with increasing sodium sorbed on the surface of the film. In [98], a linear relationship was found between the difference between the binding energies of the Sb $3d_{5/2}$ and Cl $2p$ lines and the basicity for rapidly frozen solutions of $SbCl_5$ with various Lewis bases in dichloroethane. The form of the linear relationship between the chemical shift of the O 1*s* line in metal oxides Mg, Al, Si, the Fermi level potential, and the isoelectric point was determined. When the list of oxides was extended with oxides of zinc, copper, nickel, titanium, and iron, a linear dependence of the difference in binding energies (the sum of chemical shifts) of metal and oxygen lines on the potential of the isoelectric point and the potential of the Fermi level was found [97, 98].

Another measurement option implemented at elevated pressure with synchrotron radiation is the measurement of the spectrum of a gas jet without electrical contact with the substrate and the spectrometer holder. In [99], the flow of an aerosol of nanoparticles passing through rather narrow guides (nozzles) was measured. The short mean free path of electrons in Si nanoparticles coated with SiO_2 and the sufficiently large particle size (d = 14 ± 2 nm) made it possible to neglect the elastic scattering of photoelectrons, the shift in binding energies due to quantum size effects (manifested at $d < 4$ nm), and charging.

Layered structures

To determine the concentration profile of elements in depth, etching of the sample surface with an ion beam, for example, with Ar^+, O_2^+ ions [100, 101]), ion sputtering with C_{60} clusters with a low destructive power for organic materials [102–104], profiling by a beam of ionized water clusters [105] followed by measurement by non-destructive methods of surface analysis, methods of surface ion probing (Rutherford backscattering spectroscopy, secondary ion mass spectrometry, glow discharge atomic emission spectroscopy) [106], X-ray microanalysis with an electron probe combined with calculations by the Monte Carlo [107]. In order to determine the depth profile of elements, XPS is used in XPS versions with resolution in terms of the analysis angle [108] and analysis of the shape of peaks and background [109–114].

To determine the qualitative composition in a surface layer with a thickness of more than 5–10 nm, the most applicable method is ion sputtering. This procedure has its drawbacks, such as preferential sputtering of atoms of one kind, atomic mixing and radiation-stimulated diffusion, which limits the final depth resolution. In some cases, elements are reduced to lower oxidation states.

Information depth

The depth of penetration of X-rays into the sample is much greater than the emission depth of photoelectrons. The intensity of the photoelectron beam from depth d decreases exponentially with increasing depth, according to Eq. (2) [86, 115]:

$$I = I_\infty \exp\left(-\frac{d}{\lambda\cos\theta}\right), \tag{2}$$

where λ is the electron mean free path, I_∞ is the photoemission intensity of an infinitely thick layer, and θ is the photoemission angle relative to the surface normal.

According to this equation (when integrated over the ratio d/λ), more than 95% of the photoemission comes from a surface layer with a thickness of $3\lambda\cos\theta$. The corresponding thickness is called the depth of analysis (Fig. 7).

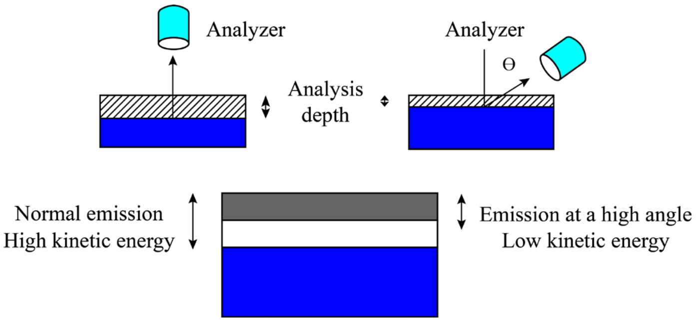

Fig. 7. Dependence of the analysis depth (information depth) on the detection angle and kinetic energy of photoelectrons [86].

To estimate the contribution of elastic and inelastic scattering of electrons in a material, two concepts are introduced into the intensity of photoelectron lines: the inelastic mean free path (λ) and the effective attenuation length [83]. The first term assumes that photoelectrons can lose energy only due to inelastic collisions, while the second term also takes into account elastic interactions, so this parameter depends on the detection angle.

Information depth is the maximum depth in the normal direction to the surface from which useful information can be obtained. It is usually given as the thickness from which a given percentage of the signal (95% or 99%) comes out and can be determined from the depth distribution function of the element, or, in general, from the mean free path of the photoelectron in the selected sample [83].

Multilayered structures

Measurements of signal intensities and determination of theoretical thicknesses for flat surfaces covered with several flat layers are described in [115]. As an example, equations are given for the intensities of two consecutive layers and a substrate [116]: outer layer (3), second layer (4), and substrate (5):

$$I_{S_1} = I_\infty(i)\left[1-\exp\left(-\frac{d_i}{-\lambda_{S_1}(i)\cos\theta}\right)\right], \tag{3}$$

$$I_{S_2} = I_\infty(j)\times \times\left[1-\exp\left(-\frac{d_2}{-\lambda_{S_2}(j)\cos\theta}\right)\right]\exp\left(-\frac{d_1}{-\lambda_{S_1}(j)\cos\theta}\right), \tag{4}$$

$$I_B(k) = I_\infty(k)\exp\left(-\frac{d_1}{\lambda_{S_1}(k)\cos\theta}\right)\exp\left(-\frac{d_2}{\lambda_{S_2}(k)\cos\theta}\right), \tag{5}$$

In the above Eqs. (3)–(5), I_B, I_{S1}, I_{S2} are the intensities of photoelectrons from the substrate, upper and lower layers, respectively, d_1 and d_2 are the thicknesses of the outer and second layers, λ_{S1} and $\lambda_{S2}(i, j, k)$ are the average the mean free path of electrons with the energies corresponding to lines i, j, k, θ is the angle of the analyzer with respect to the normal of the sample surface.

However, usually the exact values of the signal intensities from the bulk materials that make up the layers are not known. Then, for the case of a two-layer sample, the equations for the photoemission intensity of a thin film on a substrate can be written as:

$$I_{S_1}(i) = I_\infty(i)\left[1-\exp\left(-\frac{d_1}{\lambda_{S_1}(i)\cos\theta}\right)\right], \tag{6}$$

$$I_B(k) = I_\infty(k)\exp\left(-\frac{d_1}{\lambda_{S_1}(k)\cos\theta}\right). \tag{7}$$

The layer thickness d_1 is found by Eq. (8):

$$d_i = \lambda_{S_1}(i)\ln\left(\frac{I_\infty(k)I_{S_1}(i)}{I_\infty(i)I_B(k)}-1\right). \tag{8}$$

If it is difficult to theoretically predict the exact value of the signal intensity from a bulk material, then the ratio of such photoemission intensities of two different substances is found by sequentially measuring the intensity of signals from two pure materials in the same installation. The above Eq. (8) also does not take into account differences in the mean free paths, which is true for elements with a compound film with similar binding energies (and photoelectron kinetic energies), for example, a metal with an oxide film.

One of the first proposed for the analysis of thin multilayer films was the Hill equation [117]. It was used to determine the thickness of the oxide film on the silicon surface. The film thickness can be calculated by Eq. (9):

$$d_1 = \lambda_{SiO_2}\cos(\theta)\ln\left(1+\frac{\left(I_{SiO_2}/R_{SiO_2}\right)}{I_{Si}}\right). \tag{9}$$

In the presence of a large number of layers, the corresponding multipliers are introduced, as shown in the previous equations. For example, for an oxide film on a silicon surface, consisting of intermediate oxides and dioxide, Eqs. (10)–(13) were used [118]:

$$d_{SiO_2} = L_{SiO_2}\cos(\theta)\ln\left[1+\frac{\left(\dfrac{I_{SiO_2}}{R_{SiO_2}}\right)}{\left(\dfrac{I_{Si_2O_3}}{R_{Si_2O_3}}+\dfrac{I_{SiO}}{R_{SiO}}+\dfrac{I_{Si_2O}}{R_{Si_2O}}+I_{Si}\right)}\right], \tag{10}$$

$$d_{Si_2O_3} = L_{Si_2O_3}\cos(\theta)\ln\left[1+\left(\frac{I_{Si_2O_3}}{R_{Si_2O_3}I_{Si}}\right)\right], \tag{11}$$

$$d_{SiO} = L_{SiO}\cos(\theta)\ln\left[1+\left(\frac{I_{SiO}}{R_{SiO}I_{Si}}\right)\right], \tag{12}$$

$$d_{Si_2O} = L_{Si_2O}\cos(\theta)\ln\left[1+\left(\frac{I_{Si_2O}}{R_{Si_2O}I_{Si}}\right)\right]. \tag{13}$$

In Eqs. (10)–(13), for partial thicknesses of the oxide components $d_{Si_2O_x}$, the electron decay length is denoted as $L_{Si_2O_x}$, and R is the ratio of the photoemission intensities of the oxide and oxide forms, $R_0 = 0.9329$ is the ratio for SiO_2 and Si, which can be calculated from the atomic densities, attenuation length and stoichiometry (14):

$$R_{Si_2O_x} = 1+0.25\times(R_0-1). \tag{14}$$

Similarly, the concentrations of elements are calculated in structures that are a non-continuous homogeneous layer on the surface or in the depth of the sample, introducing the ratio of the layer area to the analyzed area into the calculations [119].

There is also a method [80–82, 120–122] based on the analysis of the background shape[2]. With a deeper occurrence of the component in the sample, the background signal increases in the region with a higher binding energy, and vice versa. For most metals, alloys, and oxides, the energy distribution of photoelectrons and the observed spectrum, after correction for the spectrometer transmission function, are expressed in terms of the two-parameter universal cross section according to equation (15):

$$F(E) = J(E) - \int_E^{\infty} \frac{B(E' - E)}{\left\{C + (E' - E)^2\right\}^2} J(E')dE', \tag{15}$$

where $F(E)$ is the signal intensity at a point with energy E without electron scattering (primary excitation spectrum), $J(E)$ is the experimentally measured photoelectron spectrum, E is the photoelectron binding energy, E' is also the photoelectron binding energy, but used not to determine the signal at a particular point, but as a variable for integration; B = 2866 eV and C = 1643 eV^2. For solids, such as light metals (for example, Al and Si), a simple two-parameter equation does not describe plasmon energy losses, for which a three-parameter Eq. (16) is introduced:

$$F(E) = J(E) - \\ - \int_E^{\infty} \frac{B(E' - E)}{\left\{C - (E' - E)^2\right\}^2 + D(E' - E)^2} J(E')dE'. \tag{16}$$

For thin layered structures, two-parameter Eq. (15) is written as Eq. (17):

$$F(E) = J(E) - B_1 \int_E^{\infty} \frac{(E' - E)}{\left\{1643 + (E' - E)^2\right\}^2} J(E')dE'. \tag{17}$$

In this equation, the parameter B_1 is chosen so that the intensity of the background line exactly coincides with the intensity of the experimental spectrum $J(E)$ at a distance of 30 eV from the peak maximum (thus, the background is subtracted in the range up to 30 eV towards higher binding energies beyond the peak position). Then the depth distribution of atoms can be estimated from the parameter B1 and the peak area A_p from Table 1. The attenuation depth L is determined from Eq. (18):

$$L = \frac{B_1}{B_0 - B_1} \lambda \cos\theta. \tag{18}$$

Here B_0 = 3000 eV^2, λ is the mean free path of photoelectrons, and θ is the photoemission angle with respect to the surface normal. After determining L, the depth distribution of atoms can be estimated from Table 2.

As an example of the use of Eqs. (3)–(5) or (6)–(8), the thickness of thin oxide films on transition metals may be determined [123–125]. The thickness of the oxide–hydroxide film on the surface of an alloy of niobium and zirconium (consisting of water, hydroxide, oxide, and metal layers) was determined in the same way during oxidation under atmospheric conditions with high humidity [126]. If the film consists of several oxide and hydroxide forms or contains water,

Table 1. Rules for estimating the depth distribution from the A_p/B_1 ratio, where B_1 is the adjusted parameter for the background line at a point 30 eV away from the maximum, and A_p is the area of the photoelectron peak

A_p/B_1	**Depth distribution**
≈25 eV	Uniform
>30 eV	Mostly on the surface
<20 eV	Predominantly deep in the sample

---

[2] http://www.quases.com/. Accessed April 01, 2023.

Table 2. Depth distribution estimation rules based on the attenuation depth *L*

L	**Depth distribution**
$-6\lambda_i < L < 6\lambda_i$	Uniform
$-3\lambda_i < L < 0$	Mostly on the surface
$0 < L < 3\lambda_i$	Predominantly deep in the sample

the calculation of the thickness of ultrathin films is carried out for all elements that make up the films. In [126], the fine structure of the spectra of the Zr 3*d*, Nb 3*d*, and O 1*s* lines was studied (Figs. 8–10).

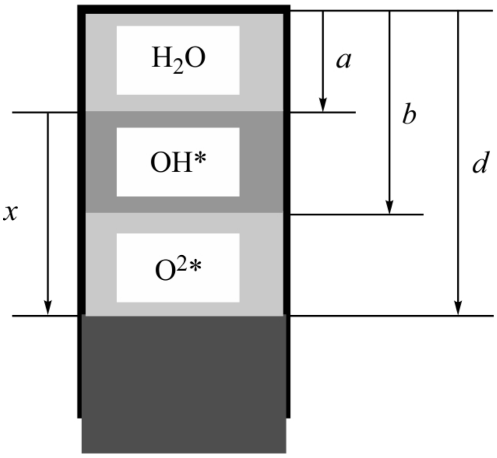

Fig. 8. Layered structure of a thin mixed oxide-hydroxide film on the surface of zirconium and niobium. The letters denote: *a* is the thickness of the water film, *b* is the total thickness of the hydroxide and water films, *d* is the total thickness of the coating layer of water, hydroxide, and oxide films, *x* is the thickness of the film corresponding to the oxidized metal [126].

Classification of samples in XPS with angular resolution

The thickness profiling of samples is possible not only with a change in the X-ray energy, but also with a change in the photoelectron detection angle. Angle-resolved XPS (AR XPS), based on the dependence of the peak intensity on the detection angle, has been used for more than 35 years as a non-destructive method for analyzing the surface structure. The accuracy, limitations, and problems of the method are presented in [127] from a theoretical point of view, and in [118] from a practical point of view, but only for a system consisting of a thin SiO_2 film on Si.

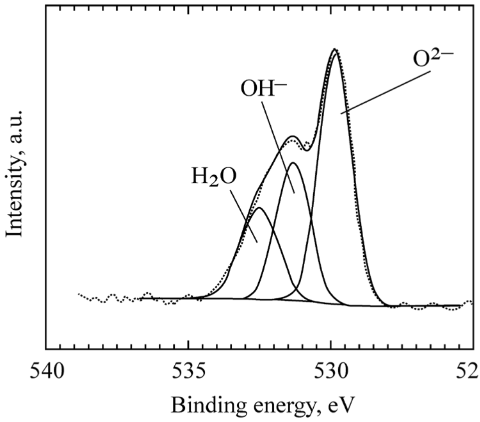

Fig. 9. Fine structure of the spectrum of the O 1*s* oxygen line with indicated peaks corresponding to oxygen in the composition of water, metal hydroxide, and oxide [126].

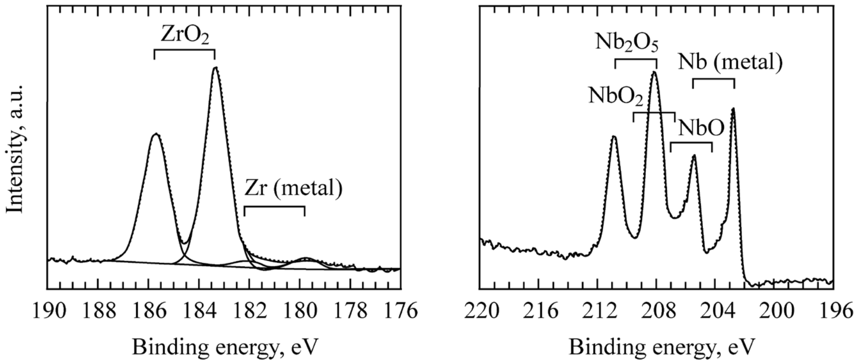

Fig. 10. Fine structure of the spectra of zirconium and niobium lines with indicated peaks corresponding to the metal and various oxide forms [126].

Angular-resolved XPS is based on quantitative expression (19) relating the measured photoelectron intensity $I_A(\theta)$ to the concentration profile $c(z)$:

$$I_A(\theta) = I_0 \int_0^\infty CF(z,\theta) f(z) \exp\left(-\frac{z}{\lambda \cos\theta}\right) dz \cong \cong I_0 \int_0^\infty f(z) \exp\left(-\frac{z}{\lambda \cos\theta}\right) dz. \quad (19)$$

In this expression, θ is the detection angle with respect to the normal, z is the depth of the layer from which photoemission occurs, $CF(z, \theta)$ is the factor responsible for elastic scattering effects, and $f(z)$ is the concentration profile of the selected element. With this designation, the signal intensity from a standard sample of known composition will be equal to $I_0\lambda\cos\theta$ at $f(z) = 1$.

According to equation (19), with a sufficient number of measurements, it is possible to obtain $f(z)$ by inverse transformation, but this procedure is extremely sensitive to errors in determining the area (intensity) of the peaks [127]. A serious limitation of the method is the need for very flat sample surfaces (to eliminate shading), which means the absence or special consideration of nanostructures on the surface [60, 127, 128] and measurements in directions that do not coincide with high symmetry directions (axes).

Depending on the complexity of the analysis, samples in XPS with angular resolution are divided into the following groups.

1. *Simple samples*. They usually consist of an element coated with an oxide film. To determine the thicknesses, the Hill equation [117] is used, which is the most accurate and simplest approach for quantifying the thickness of layers in XPS with angular resolution. If there is a significant difference between the energies of electrons from the coating layer and the substrate, the Thickogram method is used to determine the thicknesses [129].

2. *Fairly simple samples*. Multilayer samples for which a step-by-step method of thickness estimation is used [70–72]. Later, a layering method was proposed that estimates the average thickness and amount of substance in each layer. On such constructions it was impossible to determine the depth scale. Therefore, nowadays the focus is more on diffuse profiles, and not on those with clear boundaries, as was customary in the layering method. The relative amounts of one form or another of a substance or element are built on the depth scale [70, 72].

3. *Complicated samples*. Samples for which the preliminary concentration profile is unknown. For their analysis, the methods and software described in [130, 131] are used.

Concentration profile analysis

The uncertainty in calculating the concentration profile of elements in AR XPS is expressed by the depth resolution Δz. By definition, this is the thickness of the sample layer in which the calculated component concentration changes from 16% to 84% (assuming that the real sample has a sharp boundary). This choice allows us to define Δz as twice the standard deviation 2σ; when choosing 10% and 90% concentration, $\Delta z = 2.36\sigma$. If the depth profile function has an exponential rather than a Gaussian form, as in the case of electron depth attenuation, Δz (16–84%) = 1.67σ.

When analyzing the concentration profile by the AR XPS method, proceed as follows. First, the detector signal is corrected for the analyzer transmission function, since the detection efficiency depends on the kinetic energies of the electrons. Further, the cascade of secondary electrons from the high-energy side of the peak is adjusted to a straight line and such a background is subtracted. After that, a model spectrum is generated, taking into account the depth distribution of the components. Finally, the model spectrum is corrected for the experiment, which can be performed using the QUASES-Generate software [130, 131]. This software allows you to build spectra of a wide variety of concentration profiles, including buried and non-immersed layers (Frank–Van der Merwe), islands (Volmer–Weber), islands on the layer surface (Stranski–Krastanov), and exponential profile. The paper [132] gives an example of a program developed for interpreting data obtained from measurements in AR XPS.

Direct formulas and transformations are used to go from theoretical concentration profiles and phase parameters to specific line signal intensities (spectrum modeling), while inverse transformations are required to obtain concentration profiles. Inverse Laplace transforms are sensitive to fluctuations in the input intensity ratios and spectrum noise. Detailed calculations of the concentration profile, formulas, and errors in the calculations are given in [133].

To calculate the profiles of ultrathin films with sharp boundaries, the method of least entropy is successfully used. The uncertainty inherent in AR XPS is reduced as follows: each component is defined as a continuous layer (square profile) defined by three parameters (depth, thickness, and density), which fits within the limitation of parameters that can be extracted to three per element [134, 135].

The analysis is carried out separately for each component. The composition of the film is determined empirically, only after matching the individual components in depth. The composition is calculated from the ratio of concentrations, without reference to stoichiometric coefficients, which makes it possible to evaluate the changes that occur during sample preparation. The method makes it possible to take into account discrepancies, and with a smaller discrepancy than when using inverse transformations [136]. The above formulas and calculations are limitedly applicable, since real samples can have not only a rough surface, but also an inhomogeneous coating or planar (two-dimensional) inhomogeneities of the composition.

Conclusions on data processing by the AR XPS method

Based on the results of the conference on AR XPS [136], the following main conclusions were made.

First, for homogeneous films, the relative error in determining the thickness depends on the calibration of the instrument, while for inhomogeneous films, deviations are possible depending on the specifics of the distribution of components. Different thickness ranges require their own calibration by changing the effective mean free path of electrons.

Second, for thin films of unknown composition, it is difficult to switch from a qualitative dimensionless profile to a quantitative depth distribution, and for certain and limited systems, the use of AR XPS and intensity modeling leads to depth distributions that are close to real, without an exact match.

The information obtained by the AR XPS method is limited to three parameters per substance. Determination errors are the sum of limited depth resolution and unknown or variable composition of the sample, and the depth resolution $\Delta z/z$ exceeds 0.8 [136].

Small structures with a size on the order of the attenuation lengths of the radiation of characteristic electrons (or the mean free path) can be well described as smooth homogeneous layers, which mainly depends not on the structure, but on the size of the elements.

Including elastic scattering of electrons in calculations, both for modeling and for calculating experimental data, can increase the amount of structural information due to the use of photoemission angles exceeding 65°.

Further development of precise quantitative determination in AR XPS requires the development of a theory of the angular and energy distribution of photoelectrons and their exit from a solid body, including elastic scattering, which is theoretically well described, inelastic scattering that occurs in the volume of a solid body (bulk excitations), and surface excitations that occur when crossing the solid–vacuum surface [136].

Ion etch profiling

The possibilities of non-destructive layer-by-layer depth analysis in the XPS method are limited by the use of angular resolution and variation of the excitation radiation energies. The concentration profile of the components over the depth of the sample can be determined by the XPS method in the destructive variant with ion etching. A number of processes occur on the surface that change the qualitative and quantitative composition of the sample: atomic mixing in cascades of ion collisions, leading to implantation of recoil atoms, distortions of the crystal lattice during collisions, and the formation of defects (vacancies, substitutions, and agglomerates). Irradiation with ions of inert gases leads to insignificant changes, since it causes distortion of the sample only due to knocking out, displacement of atoms and selective sputtering.

Irradiation with ions of reactive gases, such as oxygen, leads to a significant change in the chemical composition and density of the sample due to the formation of new compounds. When a surface is irradiated with high energy ions, thermally activated diffusion and segregation occur [70–72].

To optimize the ion etching process, the pressure in the analysis chamber and the preparation chamber is kept as low as possible (10^{-8} Pa and below) to prevent possible contamination by sputtered atoms after etching. The area of analysis must be smaller than the spray area and be in its center. To improve depth resolution and eliminate the effect of photoemission on the sample, lines with low photoelectron kinetic energy (high binding energy) should be measured. The ion energy should not exceed 1 keV at high ion masses (heavy inert gases or cluster sources), and the ion source should produce a raster (point) beam [71, 72].

For smooth samples, etching with a large deviation from the normal (>60°) can be used; for rough samples—close to normal. The ion beam must contain a minimum amount of impurities and neutral atoms and must fall into the same region from several positions. This is possible when using multiple sources or when rotating the sample. In general, the sample to be etched should have a smooth surface, an amorphous, non-crystalline structure, consist of a single phase and elements with close sputtering yields, have good thermal and electrical conductivity, and have low counter diffusion and Gibbs segregation [137]. Atoms removed from the surface can then be analyzed by secondary ion mass spectrometry.

Features of the XPS spectra of complex objects

The size, shape and location of nanoparticles affect the experimental data obtained from XPS, causing a change in the binding energies of the peaks and Auger parameter values, the absolute and relative intensities of the peaks of various elements excited by X-rays at different energies or at different angles to the sample [50, 59].

In particular, for nanoparticles of noble metals of group VIII on SiO_2 and Al_2O_3 substrates, a positive shift in binding energies was shown compared to bulk metal samples [138].

The formation of a photo-hole as a result of photoemission affects all surrounding electrons and leads to a change in the binding energy and kinetic energy of the electron [139, 140]. The initial state contribution reflects changes in the charge density on the atom due to the chemical and geometric environment. The final state contribution arises from differences in the screening of core holes that appear during photoemission. Photoemission can lead to several types of end states. The shielding efficiency of core holes depends on a certain element (intraatomic shielding), on the environment (atom coordination number), and on the interaction with the substrate (interatomic shielding).

In the case of nanoparticles, strong electronic interaction with the substrate can make a significant contribution to interatomic screening [141]. The binding energy shift for nanoparticles on a substrate can also be contributed, to a lesser extent, by the effects of the initial state. This is charge transfer between particles and the substrate and hybridization of electronic states in them.

According to the Koopmans theorem, for a molecule with a filled shell, the binding energy of an electron in the state (orbital) *i* is equal to the orbital energy of this state with the opposite sign. This theorem makes it possible to identify the calculated energies of orbitals with ionization potentials, but it does not take into account electronic relaxation.

Intramolecular relaxation consists in the rearrangement of the remaining surrounding electrons relative to the photo-hole, leads to a decrease in energy and occurs when the molecules of a substance are hemisorbed on the surface, and their energy levels are shifted compared to a free gas or liquid. This leads to a change in the binding of the electron to the core (the effect of the initial state) and relaxation or polarization screening (the effect of the final state).

The authors of [142] indicate the following mechanisms for changing chemical shifts due to the effects of the initial state:

1) interatomic charge transfers during the interaction of a metal with an oxide (deposited layer or clusters with a substrate), which was observed during the oxidation of transition metals on oxides, with the appearance of chemical shifts of more than 1.5 eV;

2) the appearance of an electric field from the effective charges of the substrate or metal layer (charging on non-conductive substrates) and the influence of the electric field of the charge of the interface;

3) chemical shifts of the core levels of surface atoms, which include a contribution from atoms with a reduced coordination number and are caused by the rehybridization of valence levels—intraatomic charge transfer. Usually, these are small negative shifts up to −0.3 eV.

The effects of the final state, as indicated above, affect the screening of core holes after photoemission and depend on the environment of the atom. In the case of dominance of the final state effects, the shift of the binding energy is inversely proportional to the cluster size. Figure 11 shows the dependence of the binding energy on the cluster size [142].

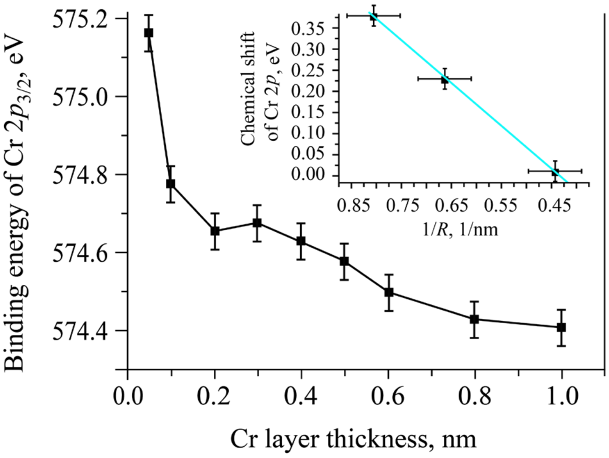

Fig. 11. Binding energy of the Cr $2p_{3/2}$ core level as a function of the thickness of the Cr layer on the $SrTiO_3$ (100) substrate. The inset shows the dependence of the chemical shift on the reciprocal radius of Cr clusters on the same substrate [142].

The initial and final state contributions can be distinguished by using the Auger parameter. The concept of the Auger parameter is based on the following assumptions:

1) for the same element in the same compound and sample, there is a fixed difference between the energies of two lines (Auger and photoelectron);

2) corrections for the charge shift of lines when measuring individual lines are insignificant, since they are not used in estimating the Auger parameter;

3) work function corrections also do not affect the value of the Auger parameter, and the vacuum energy level can be correlated with the Fermi level.

Measurement of the Auger parameter can be one of the few possible ways to identify the element and its form in the sample in the presence of a static charge on semiconductor materials and dielectrics, since it is difficult to determine the vacuum energy level in them. The Auger parameter α (20) is introduced as the difference between the kinetic energies of the two main Auger and photoelectron peaks measured on the same spectrum. The coincidence of one of the involved levels of the Auger transition with the level of photoelectron emission is not mandatory:

$$\alpha = E_{\text{kin}}(C^{'}C^{''}C^{'''}) - E_{\text{kin}}(C). \tag{20}$$

In Eq. (20), α is the Auger parameter, C', C'', C''' are the levels between which the Auger transition occurs, C is the level from which photoemission occurs, E_{kin} is the kinetic energy of the photoelectron.

Since, in the case of choosing different levels, the value of the Auger parameter could be negative, the term modified Auger parameter, α', (Eq. (21)) was introduced, corresponding to the sum of the Auger parameter α and the photon energy $h\nu$, or the binding energy E_{b} and the kinetic energy E_{kin} of the Auger electron:

$$\alpha^{'} = \alpha + h\nu = E_{\text{kin}}(C^{'}C^{''}C^{'''}) + E_{\text{b}}(C). \tag{21}$$

A detailed description of the theory with examples of how the Auger parameter changes with the chemical state of matter is given in review [139]. The paper [140] gives examples of studying samples of various compositions: alloys, modified silicon surfaces, oxides, mixed oxides, thin films, glass, metal clusters, oxide systems on substrates, interfaces between metal and organic matter, free molecules, and liquid solutions.

Calculation of signal intensities from spherical particles

For the first time, the significance of the surface structure was realized in the study of heterogeneous catalysts, which can be characterized as a powder consisting of core–shell nanoparticles. One of the reviews considering the quantitative analysis of rough surfaces [143] gives the historical development of quantitative analysis and includes formulas for correcting volumetric sensitivity factors, formulas for various layers on the surface, including continuous, carbon contamination and spherical particles, as well as formulas describing shape distortion. peak in the presence of covering layers.

For core–shell nanoparticles, several models have been developed that are applicable to powder samples. Most of these models make the following assumptions [144]:

1) for powders, an approximation of a simple sphere or even a hemisphere is given, introducing a simplification that the signal intensity from randomly located particles in the powder is equivalent to the signal intensity from a single particle;

2) elastic scattering of photoelectrons in a solid is neglected;

3) the relative mean free paths for a given photoelectron line are the same in the core and shell.

The simple sphere approximation implies that the angular distribution of photoelectrons in powders is isotropic. The other two assumptions were made in [144] and were consistent with experiments for functionalized gold nanoparticles. Divergences in the dependence of the intensity of photoemission of the particle core as a function of radius were observed only for particle sizes less than the mean free path, when the XPS method no longer becomes surface-sensitive, but volume-sensitive (Fig. 12).

Thus, the authors of the paper argue that the model of a single sphere for a powder sample is valid without any special refinements due to the random distribution of particles over the substrate and the absence of layer periodicity [144].

Attempts to quantify the photoemission intensity of spherical particles and flat shells on them were made in a number of works, for example, in one of the early detailed studies [145].

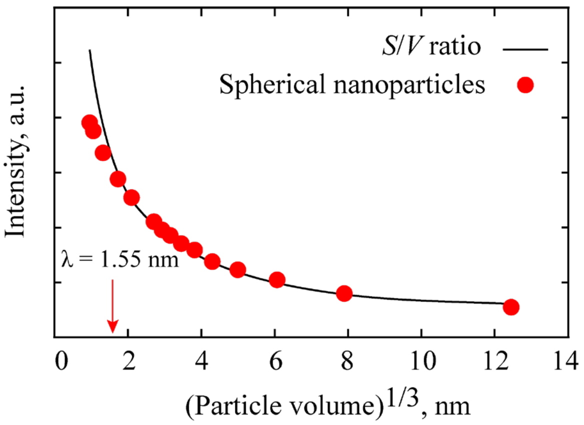

Fig. 12. Dependence of the Au 4$f_{7/2}$ line intensity as a function of the particle radius. (The solid line shows the volume-to-surface ratio $S/V = 3/R$ for a sphere. The vertical arrow indicates the mean free path of the photoelectrons in this line.)

The application of the theory described above for finding the thickness of thin films to spherical layers covering particles leads to an overestimation of the shell thickness [116, 146]. An approach to solve this problem introduces the effective layer thickness, deff, which denotes the film thickness determined by the electron analyzer. For planar thin layers, this thickness is constant in all regions of the sample; for spherical particles, it varies.

For uncoated spherical clusters, the photoemission intensity can be calculated from Eq. (22) [115]:

$$S = \pi\lambda^3\left\{x^2 + \frac{[(2x+1)\exp(-2x)-1]}{2}\right\}, \tag{22}$$

where λ is the mean free path, $x = r/\lambda$, and r is the cluster radius.

Further, the intensity of the signal from the shell can be calculated as the difference between the intensities of the signals from a spherical particle with the same diameter and a core made of the shell material. Equation (23) includes the attenuation of the core signal on a uniform shell layer, but the real thickness is different. Thus, the intensity can be approximately calculated as:

$$S(\text{core}) = \exp\left(-\frac{d}{\lambda_\text{S}}\right)\pi\lambda_\text{C} \times \\ \times\left\{x^2 + \frac{[(2x+1)\exp(-2x)-1]}{2}\right\}. \tag{23}$$

In Eq. (23), the average shell thickness and mean free paths of the corresponding photoelectrons in the core (λ_C) and shell (λ_S) are introduced, respectively.

Extended Eq. (23) in the form (24) includes additional factors [147]:

$$S(\text{core}) = \left\{\frac{[k(x)d+\lambda]}{d+\lambda}\right\}\exp\left(-\frac{d}{\lambda}\right)\pi\lambda^3 \times \\ \times\left\{x^2 + \frac{[(2x+1)\exp(-2x)-1]}{2}\right\}. \tag{24}$$

Numerical determination of the photoemission intensity of layers is given in [116] for spherical and cylindrical Si_3N_4 particles coated with a layer of hydrocarbon contamination. Particle hemispheres were divided into 9 segments of 10°, in each of which deff was determined from the average angle; photoemission intensities of the segments were multiplied by geometric correction factors proportional to the projection of the segment area and summed up (Fig. 13).

Based on the results of [115], the coefficients for spherical and cylindrical objects were obtained from geometric considerations. The equations and calculations were tested on two series of experiments with oxidized Si_3N_4 particles and aluminum foil. The possibility of such calculations was confirmed using the XPS MultiQuant software, the library of which includes all the necessary parameters. It is shown that the use of the flat layered structure model leads to an overestimation of the layer thicknesses.

For hemispherical particles on a substrate, the photoemission intensity was also calculated using Eq. (25) given in [148]:

$$\frac{I_\text{ads,normal}}{I_{\text{ads,normal},\infty}} = \pi n R^2 - 2\pi n \lambda_\text{ads}^2 \times \\ \times\left[1-\left(1+\frac{R}{\lambda_\text{ads}}\right)\exp\left(-\frac{R}{\lambda_\text{ads}}\right)\right]. \tag{25}$$

Here n is the density of particles, R is the radius, λ_ads is the mean free path of photoelectrons in the surface layer.

The intensity of the signal from the substrate, respectively, was calculated by Eq. (26):

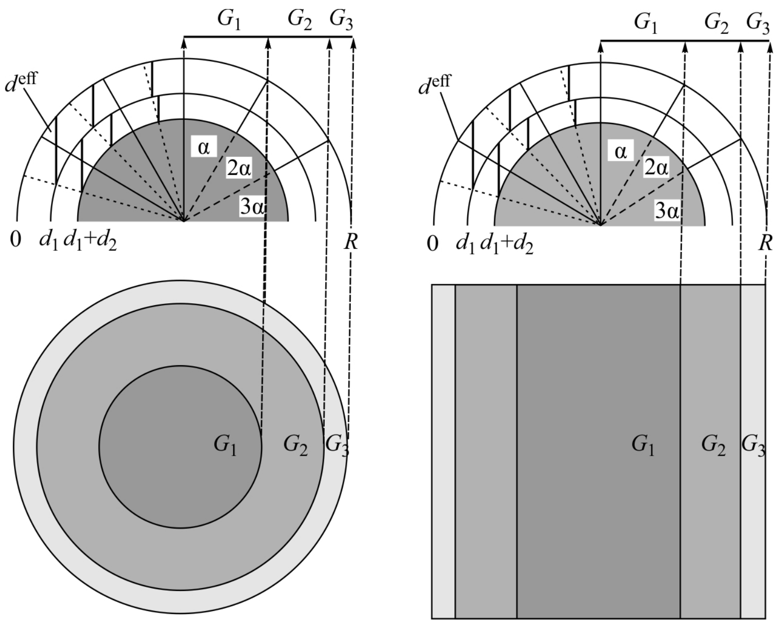

Fig. 13. Axial sections and top view of a sphere and a cylinder with two layers of coatings, made to sum the signal from the material of the core and two coating layers. Sectional sections are identical, but the shapes and ratios of the projected areas differ [115].

$$\frac{I_{\text{sub,normal}}}{I_{\text{sub,normal},\infty}} = 1 - \pi n R^2 - 2\pi n \lambda_{\text{sub}}^2 \times \left[1 - \left(1 + \frac{R}{\lambda_{\text{sub}}}\right)\exp\left(-\frac{R}{\lambda_{\text{sub}}}\right)\right]. \tag{26}$$

Both of Eqs. (25, 26) are valid only for normal detection, and for the ratio of the photoemission intensities of the same layers measured at an angle θ, the same equation looks as follows (27):

$$\frac{I_{\text{sub},\theta}}{I_{\text{sub},\theta,0}} = 1 - f(\theta, R/\lambda)\left(1 - \frac{I_{\text{sub,normal}}}{I_{\text{sub,normal},0}}\right). \tag{27}$$

The coefficient f is found from the graph according to the desired angle to the normal and the ratio R/λ. The same correction factor can be calculated by Eq. (28):

$$f(\theta, R/\lambda) = A\exp\left(-\left(\frac{R}{\lambda}\right)\Big/R'\right) + B, \tag{28}$$

where A and R' are correction parameters, B is the asymptotic value [149].

Another theoretical approach for calculating the photoemission intensities of spherical particles of the core–shell structure was proposed in [150, 151]). This model assumes that the particles have spherical symmetry and the core is in the center, the core radius is r, and the shell thickness is d. Then the signal intensity from the particle core $I(\lambda_{\text{AL}}, d, r)$ will be equal to (29):

$$I(\lambda_{\text{AL}}, d, r) = nS(\lambda_{\text{AL}}, r) \times \exp\left(-\frac{d}{\lambda_{\text{AL}}}\right) h\left(\frac{d}{\lambda_{\text{AL}}}, \frac{r}{\lambda_{\text{AL}}}\right) F_1\left(\frac{r}{\lambda_{\text{AL}}}\right), \tag{29}$$

and the explanation of the functions included in (29) can be represented by Eqs. (30)–(33):

$$S(\lambda_{\text{AL}}, r) = \frac{I_0 \lambda_{\text{AL}} \pi r^2}{n}, \tag{30}$$

$$h(\delta, \rho) = \frac{k(\rho)\delta + 1}{\delta + 1}, \tag{31}$$

$$k(\rho) = \frac{\beta_1 \rho^2 + \beta_2 \rho + 1}{\beta_1 \rho^2 + \beta_3 \rho + 1}, \tag{32}$$

$$F_1(\rho) = 1 + \frac{(2\rho+1)\exp(-2\rho)-1}{2\rho^2}. \quad (33)$$

In this model, λ_{AL} is the effective attenuation length. If the angle from the normal does not exceed 60° and the elastic scattering effects are small, the mean free path λ can be used. The atomic sensitivity factors are given by the equation for $S(\lambda_{\mathrm{AL}}, r)$, where n is the atomic density, I_0 is the signal intensity from the bulk material with a clean surface, which is proportional to the atomic sensitivity factor at a given photon energy. Further, $h(\delta,\rho)$ and $k(\rho)$ are empirically obtained functions with three given constants: $\beta_1 = 0.00288984$, $\beta_2 = 0.05135594$, $\beta_3 = 0.45982462$.

If the theoretical intensity of the photoemission of the core can be expressed as $I_{\mathrm{C}}(\lambda_{\mathrm{AL}_{\mathrm{C}}}, d, r)$, where $\lambda_{\mathrm{AL}_{\mathrm{C}}}$ is the average attenuation length of the photoelectrons corresponding to the elements of the core, then the theoretical intensity of the photoemission of the shell (34) can be described as:

$$I_{\mathrm{S}} = I(\lambda_{\mathrm{AL_S}}, d=0, r+d) - I(\lambda_{\mathrm{AL_S}}, d, r), \quad (34)$$

where $\lambda_{\mathrm{AL_S}}$ is the average attenuation length of photoelectrons from the shell. The first term corresponds to the intensity of the signal from a spherical particle of radius $(r + d)$ consisting of the shell material, the second corresponds to the intensity of the signal from a particle of radius r, of the same composition. The theoretical ratio of the intensities of photoelectron lines (35) of the shell and core will be equal, respectively [152, 153]:

$$\frac{I_{\mathrm{S}}}{I_{\mathrm{C}}} = \frac{I(\lambda_{\mathrm{AL_S}}, d=0, r+d)}{I(\lambda_{\mathrm{AL_S}}, d, r)}. \quad (35)$$

The above equations were used to calculate the shell thickness in bimetallic nanoparticles with a core consisting of gold, platinum, and rhodium, and a shell made of iron oxide [89]. This method was used to determine the growth of oxide shells on spherical silicon particles (with an initial radius of 5 nm) under normal conditions [154, 155].

The relative concentrations of oxide forms of silicon in the oxide shell can be found from Eq. (36) [150]:

$$C_{\mathrm{SiO_2}} = \frac{I_{\mathrm{S}}}{I_{\mathrm{S}} + \mu I_{\mathrm{C}}}, \quad (36)$$

where μ is the ratio of atomic densities in silicon ($4.96 \cdot 10^{22}$ cm^{-3}) and silicon dioxide ($2.27 \cdot 10^{22}$ cm^{-3}).

Software

To simulate Auger electron and X-ray photoelectron spectra and improve the accuracy of determinations in the routine analysis of samples of complex composition, the SESSA software was developed [156]. The program contains the necessary physical parameters and gives an estimate of the intensities of peaks and electronic spectra, energy and angular distributions of photoelectrons, taking into account elastic and inelastic scattering for multilayer thin films. Theoretically, the processes of formation of signal intensities on complex samples are described in a number of works, for example, [157]. Examples of use are given in [158].

In the SESSA software, the calculation of electron energy losses occurs in the infinite medium approximation, and the decrease in the peak intensity in XPS arises due to losses due to surface excitation and internal excitations (due to the appearance of a static hole in the process of photoemission) [159]. A one-step model that takes into account both of these phenomena and is based on the semi-classical dielectric response model is introduced into the QUEELS-XPS software, which performs a quantitative analysis of the intensity of the background formed by electrons with energy loss.

The Tougaard algorithm underlying the QUASES program is based on the assumption that the elastic scattering of electrons can be neglected to estimate the depth distribution from the background shape on the low-energy side of the peaks [84]. Verification of this assumption using the SESSA software on two types of samples of different Cu/Au configuration and similar Si/SiO$_2$ structure is given in [86] (Fig. 14).

In [160], the QUASES-Tougaard software was used to analyze gold nanoclusters on the surface of polystyrene. Spherical gold nanoclusters were deposited on polystyrene substrates and survey spectra were studied. The sample was presented in the form of spheres with a diameter of $2R$ with surface coverage f_1. For quantitative calculations, the spheres were conditionally divided into 9 coaxial cylinders of equal area and different heights (Fig. 15).

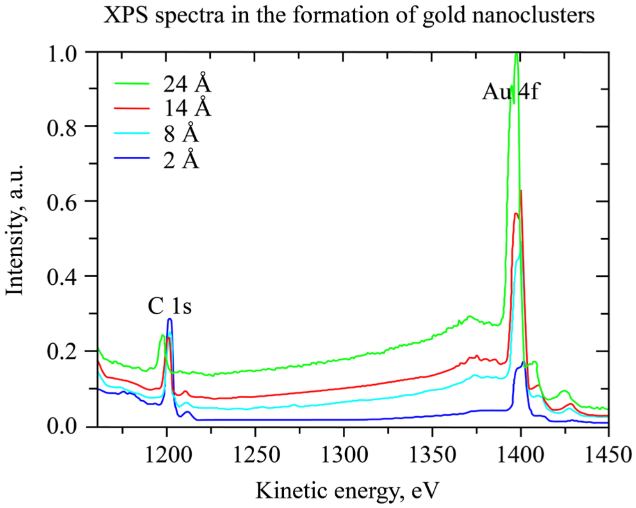

Fig. 14. X-ray photoelectron spectra obtained from samples with different effective thicknesses of the gold layer (from 0.2 to 2.4 nm). As the thickness of the gold layer increases, the photoelectron peaks C 1*s* and Au 4*f* shift, and the intensity of the peaks and the background of inelastically scattered electrons increases [160].

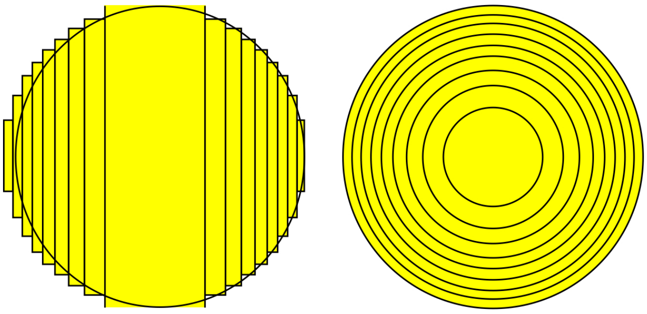

Fig. 15. Separation of spheres of radius 2*R* into 9 coaxial cylindrical shells with equal area and different heights in vertical and lateral projections was performed to calculate the total signal intensity [160].

In [86], the program generated spectra for samples containing gold and copper in the form of various compounds and alloys, as well as for silicon and silicon dioxide, with different distributions over the depth and area of the sample. In [161], the surface was coated by deposition of vanadium oxide and cerium oxide on aluminum oxide substrates, and cerium oxide and cadmium sulfide on titanium oxide substrates. The experimental spectra obtained were in good agreement with those generated in the program.

Overcoming the challenges of nanoparticle analysis

The main parameters studied in the characterization of nanoparticles are the size and shape, qualitative and quantitative composition, the size distribution function of nanoparticles, the degree of aggregation, surface charge and surface area, and the chemical composition of the surface of particles of the core–shell type [3, 51, 162, 163]. The average size, size distribution and organic ligands present on the surface of the particles can influence the properties and possible applications of the nanoparticles. In addition, the structure of nanoparticles and their chemical composition should be investigated both at the first stage after the synthesis of nanoparticles and for a sufficiently long time after synthesis due to the influence of the aging effect of nanoparticles [3, 51].

The results of methods for measuring the physicochemical parameters of nano-objects significantly affect the prediction of the use of these materials for commercial purposes. At present, the scientific community is faced with t he task of further improving the accuracy and resolution of many methods for the analysis of nanoparticles and nanomaterials [49, 51, 162–165]. However, there are significant problems in the analysis of nanomaterials due to the lack of suitable standard materials for calibrating analytical instruments, difficulties associated with sample preparation for analysis and interpretation of data *in situ* and *operando*, especially in large-scale production, as well as their analysis in complex matrices [49, 164].

Obtaining a sufficiently complete picture of the properties of nanomaterials requires the use of a group of complementary instrumental methods of analysis [3, 44, 63–67]. Of particular interest are ultrafast spectral and diffraction methods, which make it possible to understand the connection between the elements of the structure–dynamics–function triad. Significant success in their application to the study of nano-objects is associated with the development of synchrotron radiation technologies and free electron lasers, which provide X-ray sources of high brightness and high temporal resolution [53–56]. As applied to nano-objects, the use of ultrashort X-ray pulse diffraction makes it possible to study heterogeneous processes at the solid–liquid surface interface, which includes the preparation of thin liquid films and XPS measurements at high (atmospheric) pressure [60, 61, 91, 94, 165], structural dynamics in extreme conditions, which makes it possible to provide information about the behavior of nano-objects in states far from equilibrium.

CONCLUSIONS

The review depicted a number of methods for the synthesis and preparation of nanomaterials with a wide range of their applications. With the expansion of the production of nanoparticles, more reliable rapid methods of analysis will be required. Currently, the analysis is focused not only on the characterization of the core of nanoparticles, but also on surface ligands that affect their physical properties. Due to the difficulties with reproducibility and reliability in determining the physicochemical parameters of nanomaterials, a combined approach is required to find their required properties. Some issues in the field of nanomaterials research remain unresolved. This review describes the role of a number of methods for characterizing nanomaterials, highlights their advantages and limitations, as well as the possibilities of effective combination, presents both general and modern operando methods that are used to monitor the formation kinetics and properties of nanoparticles.

XPS is the most widely used analytical method for chemical surface analysis and is also used to characterize nanoparticles and nanomaterials. Its physical principle is based on the photoelectric effect. XPS is a powerful quantitative method useful for elucidating the electronic structure, elemental composition, and oxidation states of elements in a material. It can also analyze ligand exchange interactions, nanoparticle surfaces, and core–shell structures.

Compared to microscopy methods such as TEM and TEM/EELS (electron energy loss spectroscopy in a transmission electron microscope), which use transverse spatial resolution to identify elements in the transmission direction, XPS examines the composition of a material by analyzing the spectrum of ejected electrons. As an added benefit, XPS provides depth information similar to the size of nanoparticles (up to 10 nm deep from the surface) and does not cause significant damage to samples. Two disadvantages of XPS are the need for careful sample preparation (requires a dry solid form without contamination) and data interpretation.

XPS is a reliable and useful tool for the quantitative study of proteins as well as peptides adsorbed at interfaces. The method can also characterize the molecular interface. Chemical information from the surface of nanoparticles analyzed by XPS can be used to estimate the thickness of nanoparticle coatings. XPS also provides information about their dielectric properties by recording the behavior of nanomaterials during charging/discharging.

The advantage of the high sensitivity of XPS should be emphasized, since each element has a certain characteristic set of peaks in the photoelectron spectrum at kinetic energies determined by the photon energy and the corresponding binding energies, and the intensity of the peaks depends on the concentration of the corresponding element.

Originally existing as a method for carrying out measurements and research under conditions of ultrahigh vacuum, XPS has also been developed in application to processes and objects that occur and exist at higher pressures comparable to atmospheric pressure. Therefore, the range of possible measurement samples has expanded to include solutions (for example, solutions of nanoparticles), thin liquid films, and biological objects. The changes affected the design of the device and also affected the radiation sources. It became possible to use synchrotron and ultraviolet sources, access to the measurement of new spectra, for example, the spectra of the valence band, and the determination of the corresponding characteristics of matter. One of the main problems solved by the XPS method is the measurement of the composition and structure of layered samples and samples of a complex, inhomogeneous structure (spherical particles) and the determination of the concentration profile of elements in them. Another problem associated with quantitative analysis is the technique for subtracting non-linear background, especially under complex spectra of samples containing several different overlapping lines. To solve these problems, special software has been created, the principle of which is to approximate the model spectrum for the proposed structure of the sample to the experimental spectrum.

However, despite all the difficulties and problems associated with the analysis of nanomaterials, XPS successfully makes it possible to determine the charge states of elements, the composition and structure of the surface of various samples (and the list of possible samples and methods for their analysis is constantly expanding) by performing *in situ* and *operando* analysis. In combination with methods that make it possible to study the physical structure and structure of samples, the XPS method is able to provide sufficient information for the processes of obtaining and using nano-objects.

Acknowledgments

The work was supported by the Russian Foundation for Basic Research grant No. 20-02-00146 A.

Authors' contributions

A.A. Ischenko *– writing the main part of the review, editing the text, combining materials from different authors, and assembling a full text.*

M.A. Lazov *– writing the main part of the review, text design and preparation for publication.*

E.V. Mironova *– consultations and text additions on analytical research methods of various objects, editing and formatting the text.*

A.Yu. Putin *– consultations and text additions on the technology of obtaining nanomaterials and their physical properties.*

A.M. Ionov *– consultations and text additions on the topic of nanomaterials research by the XPS and on the basics and advanced theory of the XPS method.*

P.A. Storozhenko *– consultations and text additions on the topic of studying the properties of nanomaterials by various physical and physicochemical methods.*

The authors declare no conflicts of interest.

REFERENCES

1. Eliseev A.A., Lukashin A.V. *Funktsional'nye nanomaterialy* (Tretyakov Yu.D. (Ed.). Functional Nanomaterials). Moscow: FIZMATLIT; 2010. 456 c. (in Russ.). ISBN 978-5-9221-1120-1

2. Chaudhuri R.G., Paria S. Core/Shell Nanoparticles: Classes, Properties, Synthesis Mechanisms, Characterization, and Applications. *Chem. Rev.* 2012;112(4):2373–2433. https://doi.org/10.1021/cr100449n

3. Ischenko A.A., Fetisov G.V., Aslanov L.A. *Nanosilicon: properties, synthesis, applications, methods of analysis and control*. London: CRC, Taylor & Francis; 2015. 727 p.

[Original Russian Text: Ischenko A.A., Fetisov G.V., Aslanov L.A. *Nanokremnii: svoistva, poluchenie, primenenie, metody issledovaniya i kontrolya* (*Nanosilicon: properties, synthesis, applications, methods of analysis and control*). Moscow: FIZMATLIT; 2013. 614 p. (in Russ.). ISBN 978-5-9221-1369-4]

4. Borisenko V.E. Nanoelectronics – a basis of information systems for the 21st century. *Sorosovskii Obrazovatel'nyi Zhurnal = Soros Educational Journal*. 1997;(5):100–104 (in Russ.). URL: http://www.pereplet.ru/nauka/Soros/pdf/9705_100.pdf

5. Osetrov A.Yu., Vigdorovich V.I. Modern nano technologies. State, problems, and perspectives. *Vestnik Tambovskogo universiteta. Seriya Estestvennye i tekhnicheskie nauki = Tambov University Reports. Series: Natural and Technical Sciences*. 2013;18(5):2371–2374 (in Russ.).

6. Demikhovskii V.Ya. Quantum wells, wires and dots. *Sorosovskii Obrazovatel'nyi Zhurnal = Soros Educational Journal.* 1997;(5):80–86 (in Russ.). URL: http://window.edu.ru/resource/993/20993/files/9705_080.pdf

7. Shik A.Ya. Guantum wires. *Sorosovskii Obrazovatel'nyi Zhurnal = Soros Educational Journal*. 1997;(5):87–92 (in Russ.). URL: http://pereplet.ru/nauka/Soros/pdf/9705_087.pdf

8. Peter Ju., Kardona Yu.M. *Osnovy fiziki poluprovodnikov* (*Fundamentals of semiconductor physics*: transl. from Engl). Moscow: FIZMATLIT; 2002. 560 p. (in Russ.). ISBN 5-9221-0268-0

9. Peter Y., Cardona Yu.M. *Fundamentals of semiconductors: Physics and materials properties* (Graduate texts in physics). 4th ed. Berlin-Heidelberg: Springer-Verlag; 2010. 775 p. ISBN 978-364-200-709-5

10. Hamaguchi C. *Basic semiconductors physics*. 2nd ed. Berlin Heidelberg: Springer-Verlag; 2010. 570 p. ISBN 978-3-642-03302-5

11. Baer D.R., Amonette J.E., Engelhard M.H., Gaspar D.J., Karakoti A.S., Kuchibhatla S., Nachimuthu P., Nurmi J.T., Qiang Y., Sarathy V., Seal S., Sharma A., Tratnyek P.G., Wang C.-M. Characterization challenges for nanomaterials. *Surf. Interface Anal.* 2008;40(3–4):529–537. https://doi.org/10.1002/sia.2726

12. Koole R., Groeneveld E., Vanmaekelbergh D., Meijerink A., de Mello Donegá C. Size Effects on Semiconductor Nanoparticles. In: de Mello Donegá C. (Eds.) *Nanoparticles*. Berlin, Heidelberg: Springer; 2014. 299 p. https://doi.org/10.1007/978-3-662-44823-6_2

13. Sun C.Q. *Relaxation of the Chemical Bond. Skin Chemisorption Size Matter ZTP Mechanics H2O Myths*. Singapore: Springer Science & Business Media; 2014. 807 p. https://doi.org/10.1007/978-981-4585-21-7

14. Attia Y., Samer M. Metal clusters: New era of hydrogen production. *Renew. Sust. Energ. Rev.* 2017;79:878–892. https://doi.org/10.1016/j.rser.2017.05.113

15. Jin R., Li G., Sharma S., Li Y., Du X. Toward Active-Site Tailoring in Heterogeneous Catalysis by Atomically Precise Metal Nanoclusters with Crystallographic Structures. *Chem. Rev.* 2021;121(2):567–648. https://doi.org/10.1021/acs.chemrev.0c00495

16. Liu L., Corma A. Metal catalysts for heterogeneous catalysis: from single atoms to nanoclusters and nanoparticles. *Chem. Rev.* 2018;118(10):4981–5079. https://doi.org/10.1021/acs.chemrev.7b00776

17. Cuenya B.R. Synthesis and catalytic properties of metal nanoparticles: Size, shape, support, composition, and oxidation state effects. *Thin Solid Films.* 2010;518(12):3127–3150. https://doi.org/10.1016/j.tsf.2010.01.018

18. Wang H., Wang L., Lin D., Feng X., Niu Y., Zhang B., Xiao F.S. Strong metal–support interactions on gold nanoparticle catalysts achieved through Le Chatelier's principle. *Nat. Catal.* 2021;4(5):418–424. https://doi.org/10.1038/s41929-021-00611-3

19. Chen M.S., Goodman D.W. Structure–activity relationships in supported Au catalysts. *Catal. Today*. 2006;111(1–2):22–33. https://doi.org/10.1016/j.cattod.2005.10.007

20. Cheng N., Zhang L., Doyle-Davis K., Sun X. Single-Atom Catalysts: From Design to Application. *Electrochem. Energ. Rev.* 2019;2(4):539–573. https://doi.org/10.1007/s41918-019-00050-6

21. Rong H., Ji S., Zhang J., Wang D., Li Y. Synthetic strategies of supported atomic clusters for heterogeneous catalysis. *Nat. Commun.* 2020;11:5884(14 p.). https://doi.org/10.1038/s41467-020-19571-6

22. Zhang Y., Yang J., Ge R., Zhang J., Cairney J.M., Li Y., Zhu M., Li S., Li W. The effect of coordination environment on the activity and selectivity of single-atom catalysts. *Coord. Chem. Rev*. 2022;461:214493(48 p.). https://doi.org/10.1016/j.ccr.2022.214493

23. Sankar M., He Q., Engel R.V., Sainna M.A., Logsdail A.J., Roldan A., Willock D.J., Agarwal N., Kiely C.J., Hutchings G.J. Role of the support in gold-containing nanoparticles as heterogeneous catalysts. *Chem. Rev.* 2020;120(8):3890–3938. https://doi.org/10.1021/acs.chemrev.9b00662

24. Jiang Zh., Zhang W., Jin L., Yang X., Xu F., Zhu J., Huang W. Direct XPS Evidence for Charge Transfer from a Reduced Rutile TiO_2(110) Surface to Au Clusters. *J. Phys. Chem. C.* 2007;111(33): 12434–12439. https://doi.org/10.1021/jp073446b

25. Haruta M. Size- and support-dependency in the catalysis of gold. *Catal. Today*. 1997;36(1):153–166. https://doi.org/10.1016/S0920-5861(96)00208-8

26. Kung M.C., Lee J.H., Chu-Kang A., Kung H.H. Selective reduction of NO_x by propene over Au/γ-Al_2O_3 catalysts. *Stud. Surf. Sci. Catal.* A. 1996;101:701–707. https://doi.org/10.1016/s0167-2991(96)80281-3

27. Ueda A., Oshima T., Haruta M. Reduction of nitrogen monoxide with propene in the presence of oxygen and moisture over gold supported on metal oxides. *Appl. Catal. B*. 1997;12(2–3):81–93. https://doi.org/10.1016/s0926-3373(96)00069-0

28. Sanchez R.M.T., Ueda A., Tanaka K., Haruta M. Selective oxidation of CO in hydrogen over gold supported on manganese oxide. *J. Catal.* 1997;168(1):125–127. https://doi.org/10.1006/jcat.1997.1636

29. Smolentseva E.V., Bogdanchikova N.E., Simakov A.V., Pestryakov A.N., Tuzovskaya I.V., Avalos M., Farias M., Diaz A. Influence of modifyning agent on physical and chemical properties and catalytic properties of gold zeolite catalysts. *Izvestiya Tomskogo politekhnicheskogo universiteta = Bulletin of the Tomsk Polytechnic University.* 2005;308(4):93–98 (in Russ.).

30. Shubhashish S., Karasik S.J., Posada L.F., Amin A.S., Achola L.A., Nisly N., Willis W.S., Suib S.L. Syntheses of gold supported on metal oxides and their application in organic transformations. *Microporous Mesoporous Mater.* 2022;336:111888(p.). https://doi.org/10.1016/j.micromeso.2022.111888

31. Lin J.N., Chen J.H., Hsiao C.Y., Kang Y.-M., Wan B. Gold supported on surface acidity modified Y-type and iron/Y-type zeolite for CO-oxidation. *Appl. Catal. B.* 2002;36(1):19–29. https://doi.org/10.1016/s0926-3373(01)00276-4

32. Espinos J.P., Morales J., Barranco A., Caballero A., Holgado J.P., Gonzalez-Elipe A. Interface Effects for Cu, CuO, and Cu_2O Deposited on SiO_2 and ZrO_2. XPS Determination of the Valence State of Copper in Cu/SiO_2 and Cu/ZrO_2 Catalysts. *J. Phys. Chem.* B. 2002;106(27):6921–6929. https://doi.org/10.1021/jp014618m

33. Mazalova V.N., Kravtsova A.N., Soldatov A.V. *Nanoklastery. Rentgenospektral'nye issledovaniya i komp'yuternoe modelirovanie* (*Nanoclusters. X-ray spectral studies and computer modeling*). Moscow: FIZMATLIT; 2013. 184 p. (in Russ.).

34. Sacher E. Asymmetries in Transition Metal XPS Spectra: Metal Nanoparticle Structure, and Interaction with the Graphene-Structured Substrate Surface. *Langmuir*. 2010;26(6):3807–3814. https://doi.org/10.1021/la902678x

35. Alov N.V., Kutsko D.M., Bordo K.V. Ion-beam reduction of the surface of higher oxides of molybdenum and tungsten. *J. Surf. Investig*. 2008;(2):184–188. https://doi.org/10.1134/S1027451008020043

[Original Russian Text: Alov N.V., Kutsko D.M., Bordo K.V. Ion-beam reduction of the surface of higher oxides of molybdenum and tungsten. *Poverkhnost'. Rentgenovskie, sinkhrotronnye i neitronnye issledovaniya = Journal of Surface Investigation. X-Ray, Synchrotron and Neutron Techniques*. 2008;(3):17–22 (in Russ.).]

36. Alov N.V., Kutsko D.M. Surface composition modification of tungsten higher oxide upon He^+ ion bombardment. *J. Surf. Investing.* 2008;6(2):225–228. https://doi.org/10.1134/S1027451012030032

[Original Russian Text: Alov N.V., Kutsko D.M. Surface composition modification of tungsten higher oxide upon He^+ ion bombardment. P*overkhnost'. Rentgenovskie, sinkhrotronnye i neitronnye issledovaniya = Journal of Surface Investigation. X-Ray, Synchrotron and Neutron Techniques*. 2012;(3):38–41 (in Russ.).]

37. Alov N., Kutsko D., Spirovova I., Bastl Z. XPS study of vanadium surface oxidation by oxygen ion bombardment. *Surf. Sci*. 2006;600(8):1628–1631. https://doi.org/10.1016/j.susc.2005.12.052

38. Alov N.V., Kutsko D.M. Ion Beam Reduction of the Surface of Higher Niobium Oxide. *J. Surf. Investing*. 2010;4(2):232–235. https://doi.org/10.1134/S1027451010020096

[Original Russian Text: Alov N.V., Kutsko D.M. Ion Beam Reduction of the Surface of Higher Niobium Oxide. *Poverkhnost'. Rentgenovskie, sinkhrotronnye i neitronnye issledovaniya = Journal of Surface Investigation. X-Ray, Synchrotron and Neutron Techniques*. 2010;(3):66–70 (in Russ.).]

39. Khanuja M., Sharma H., Mehta B.R., Shivaprasad S.M. XPS depth-profile of suboxide distribution at the native oxide/Ta interface. *J. Electron. Spectrosc. Relat. Phenom*. 2009;169(1):41–45. https://doi.org/10.1016/j.elspec.2008.10.004

40. Alov N.V., Kutsko D.M. Ion Beam Reduction of the Surface of Tantalum Higher Oxide. *J. Surf. Investing.* 2011;5(2):259–262. https://doi.org/10.1134/S1027451011030037

[Original Russian Text: Alov N.V., Kutsko D.M. Ion Beam Reduction of the Surface of Tantalum Higher Oxide. *Poverkhnost'. Rentgenovskie, sinkhrotronnye i neitronnye issledovaniya = Journal of Surface Investigation. X-Ray, Synchrotron and Neutron Techniques*. 2011;(3):59–62 (in Russ.).]

41. Pradeep T., Anshup. Noble metal nanoparticles for water purification: A critical review. *Thin Solid Films.* 2009;517(24):6441–6478. https://doi.org/10.1016/j.tsf.2009.03.195

42. Kuzmicheva G.M. Nanosized phases with titanium(IV) oxides. Preparation. Characterisation. Properties. *Fine Chem. Technol*. 2015;10(6):5–36 (in Russ.).

43. Siciliano P. Preparation, characterisation and applications of thin films for gas sensors prepared by cheap chemical method. *Sens. Actuat. B: Chem*. 2000;70(1–3):153–164. https://doi.org/10.1016/s0925-4005(00)00585-2

44. Antipin I.S., *et al*. Functional supramolecular systems: design and applications. *Russ. Chem. Rev*. 2021;90(8):895–1107. https://doi.org/10.1070/RCR5011

45. Ding P., Chen L., Wei C., Zhou W., Li C., Wang J., Wang M., Guo X., Stuart M.A.C., Wang J. Efficient Synthesis of Stable Polyelectrolyte Complex Nanoparticles by Electrostatic Assembly Directed Polymerization. *Macromol. Rapid Comm*. 2021;42(4):2000635(1–9). https://doi.org/10.1002/marc.202000635

46. Stuart M.A.C. Supramolecular perspectives in colloid science. *Colloid Polym, Sci*. 2008;286(8–9):855–864. https://doi.org/10.1007/s00396-008-1861-7

47. Mourdikoudis S., Pallares R.M., Thanh N.T.K. Characterization techniques for nanoparticles: comparison and complementarity upon studying nanoparticle properties. *Nanoscale*. 2018;10(27):12871–12934. https://doi.org/10.1039/C8NR02278J

48. Grainger D.W., Castner D.G. Nanobiomaterials and nanoanalysis: opportunities for improving the science to benefit biomedical technologies. *Adv. Mater*. 2008;20(5):867–877. https://doi.org/10.1002/adma.200701760

49. Montaño M.D., Ranville J., Lowry G.V., Blue J., Hiremath N., Koenig S., Tuccillo M.E., Gardner S.P. *Detection and Characterization of Engineered Nanomaterials in the Environment: Current State-of-the-Art and Future Directions*. Washington, DC: U.S. Environmental Protection Agency Office of Research and Development. 2020.186 p. URL: https://clu-in.org/download/techfocus/nano/Nano-Gardner-600-r-14-244.pdf

50. Baer D.R., Engelhard M.H. XPS analysis of nanostructured materials and biological surfaces. *J. Electron Spectrosc*. 2010;178–179:415–432. https://doi.org/10.1016/j.elspec.2009.09.003

51. Koroleva M.Yu., Yurtov E.V. Ostwald ripening in macro- and nanoemulsions. *Uspekhi khimii = Russ. Chem. Rev.* 2021;90(3):293–323 https://doi.org/10.1070/RCR4962

52. Neoh K.G., Li M., Kang E.-T. Characterization of Nanomaterials/Nanoparticles. In: Kishen A. (Ed.). *Nanotechnology on Endodontics: Current and Potential Clinical Applications*. Switzerland: Springer International Publishing; 2015. P. 23–44. https://doi.org/10.1007/978-3-319-13575-5_3

53. Ischenko A.A., Weber P.M., Miller R.J.D. Transient structures and chemical reaction dynamics. *Russ. Chem. Rev.* 2017;86(12):1173–1253. https://doi.org/10.1070/RCR4754

54. Ischenko A.A., Fetisov G.V. *Structural dynamics*: in 2 v. Moscow: FIZMATLIT; 2021. V. 1. 486 p. ISBN 978-5-9221-1936-9. V. 2. 467 p. ISBN 978-5-9221-1937-5 (in Russ.).

55. Nguyen M.T., Nefedov V.I., Chekalkin N.S., Kozlovsky I.V., Malafeev A.V., Mirolyubova N.A., Nazarenko M.A. On the integration of the methods of forming and research of images of objects against the background of noises and interference. *Russ. Technol. J.* 2020;8(2):33–42 (in Russ.). https://doi.org/10.32362/2500-316X-2020-8-2-33-42]

56. Aseyev S.A., Ischenko A.A., Kompanets V.O., Kochikov I.V., Malinovskii A.L., Mironov B.N., Poydashev D.G., Chekalin S.V., Ryabov E.A. Study of the Processes Induced by Femtosecond Laser Radiation in Thin Films and Molecular-Cluster Beams Using Ultrafast Electron Diffraction. *Crystallogr. Rep.* 2021;66(6):1031–1037. https://doi.org/10.1134/S106377452106002X

57. Baer D.R. Guide to making XPS measurements on nanoparticles. *J. Vac. Sci. Technol. A*. 2020;38(3):031201. https://doi.org/10.1116/1.5141419

58. Krishna D.N.G., Philip J. Review on surface-characterization applications of X-ray photoelectron spectroscopy (XPS): Recent developments and challenges. *Appl. Surface Sci. Adv*. 2022;12:100332(30 p). https://doi.org/10.1016/j.apsadv.2022.100332

59. Baer D.R., Gaspar D.J., Nachimuthu P., Techane S., Castner D. Application of surface chemical analysis tools for characterization of nanoparticles. *Anal. Bioanal. Chem.* 2010;396(3):983–1002. https://doi.org/10.1007/s00216-009-3360-1

60. Saveleva V.A., Savinova E.R. Insights into electrocatalysis from ambient pressure photoelectron spectroscopy. *Curr. Opin. Electrochem*. 2019;17:79–89. https://doi.org/10.1016/j.coelec.2019.03.016

61. Arble C., Jia M., Newberg J.T. Lab-based ambient pressure X-ray photoelectron spectroscopy from past to present. *Surf. Sci. Rep*. 2018;7(2):37–57. https://doi.org/10.1016/j.surfrep.2018.02.002

62. Vudraf D., Delchar T. *Sovremennye metody issledovaniya poverkhnosti* (*Modern Methods of Surface Research*): transl. from Eng. Moscow: Mir; 1989. 564 p. (in Russ.).

63. Alov N.V., Lazov M.A., Ischenko A.A. X-ray photoelectron spectroscopy. In: *Analytical Chemistry*: textbook: in 3 v. V. 2. *Instrumental methods of analysis. Part 1*. IschenkoA.A. (Ed.). Chapter 3. P. 191–229. Moscow: FIZMATLIT; 2019. 472 p. (in Russ.). ISBN 978-5-9221-1866-8

64. Shtykov S.N. Chemical Analysis in Nanoreactors: Main Concepts and Applications. *J. Analyt. Chem.* 2002;57(10):859–868. https://doi.org/10.1023/A:1020410605772

[Original Russian Text: Shtykov S.N. Chemical Analysis in Nanoreactors: Main Concepts and Applications. *Zhurnal analiticheskoi khimii*. 2002;57(10):1018–1028 (in Russ.).]

65. Troyan V.I., Pushkin M.A., Borman V.D., Tronin V.N. *Fizicheskie osnovy metodov issledovaniya nanostruktur i poverkhnosti tverdogo tela* (*Physical foundations of methods for studying nanostructures and solid surface*). Borman V.D. (Ed.). Moscow: MEPhI; 2008. 260 p. (in Russ).

66. Shtykov S.N. Nanoanalytics: definitions, classification, history and primary advances. In: *Nanoanalytics: Nanoobjects and Nanotechnologies in Analytical Chemistry. Pt. I: Nanoanalytics: Concepts, Elements, and Peculiarities.* Shtykov S.N. (Ed.). Berlin: De Gruyter; 2018. P. 3–52. https://doi.org/10.1515/9783110542011-001

67. Shtykov S.N. Nanoanalytics. In: *Analytical Chemistry*: textbook: in 3 v. V. 3. I*nstrumental methods of analysis. Part 2*; Ischenko A.A. (Ed.). Chapter 2. P. 96–128. Moscow: FIZMATLIT; 2020. 504 p. (in Russ.). ISBN 978-5-9221-1867-5

68. Oswald S. X-ray Photoelectron Spectroscopy in Analysis of Surfaces. In: *Encyclopedia of Analytical Chemistry: Applications, Theory and Instrumentation*. John Wiley & Sons; 2013. P. 1–49. https://doi.org/10.1002/9780470027318.a2517

69. Crist B.V. XPS in industry – Problems with binding energies in journals and binding energy databases. *J. Electron Spectrosc.* 2019;231:75–87. https://doi.org/10.1016/j.elspec.2018.02.005

70. Greczynski G., Hultman L. X-ray photoelectron spectroscopy: Towards reliable binding energy referencing. *Prog. Mater. Sci*. 2020;107:100591(46 p.). https://doi.org/10.1016/j.pmatsci.2019.100591

71. Bolli E., Kaciulis S., Mezzi A. ESCA as a Tool for Exploration of Metals' Surface. *Coatings*. 2020;10(12):1182(27 p.). https://doi.org/10.3390/coatings10121182

72. Hofmann S. *Auger- and X-ray Photoelectron Spectroscopy in Materials Science*. Berlin Heidelberg: Springer-Verlag; 2013. 527 p. https://doi.org/10.1007/978-3-642-27381-0

73. Hűfner S. *Photoelectron Spectroscopy: Principles and Applications*. Berlin Heidelberg: Springer-Verlag; 2003. 661 p.

74. Baer D.R., Artyushkova K., Brundle C.R., Castle J., Engelhard M., Gaskell K., Grant J., Haasch R., Linford M.R., Powell C., Shard A., Sherwood P., Smentkowski V. Practical guides for X-ray photoelectron spectroscopy: First steps in planning, conducting, and reporting XPS measurements. *J. Vac. Sci. Technol. A.* 2019;37(3):031401. https://doi.org/10.1116/1.5065501

75. Schalm O., Patelli A., Storme P., Crabbé A., Voltolina S., Feyer V., Terryn H. A dataset of high-resolution synchrotron X-ray photoelectron spectra of tarnished silver-copper surfaces before and after reduction with a remote helium plasma at atmospheric pressure. *Elsevier, Data in Brief*. 2021;35:106872. https://doi.org/10.1016/j.dib.2021.106872

76. Bagus P., Ilton E., Nelin C. The interpretation of XPS spectra: Insights into materials properties. *Surf. Sci. Rep.* 2013;68(2):273–304. https://doi.org/10.1016/j.surfrep.2013.03.001

77. Powell C.J. Improvements in the reliability of X-ray photoelectron spectroscopy for surface analysis. *J. Chem. Educ.* 2004;81(12):1734–1741. https://doi.org/10.1021/ed081p1734

78. Powell C.J., Jablonski A. Surface sensitivity of X-ray photoelectron spectroscopy. *Nucl. Instrum. Meth. A.* 2009;601(1–2):54–65. https://doi.org/10.1016/j.nima.2008.12.103

79. Shard A.G. Detection limits in XPS for more than 6000 binary systems using Al and Mg Kα X-rays. *Surf. Interface Anal*. 2014;46(3):175–185. https://doi.org/10.1002/sia.5406

80. Jo M. Direct, simultaneous determination of XPS background and inelastic differential cross section using Tougaard's algorithm. *Surf. Sci.* 1994;320(1–2):191–200. https://doi.org/10.1016/0039-6028(94)91270-X

81. Seah M.P. Background subtraction: I. General behaviour of Tougaard-style backgrounds in AES and XPS. *Surf. Sci.* 1999;420(2–3):285–294. https://doi.org/10.1016/S0039-6028(98)00852-8

82. Végh J. The Shirley background revised. *J. Electron Spectrosc*. 2006;151(3):159–164. https://doi.org/10.1016/j.elspec.2005.12.002

83. Briggs D., Grant J.T. *Surface analysis by Auger and X-ray photoelectron spectroscopy*. Chichester: IM Publications; 2003. 899 p.

84. Powell C.J. New Data Resources and Applications for AES and XPS (Papers from 6th International Symposium on Practical Surface Analysis (PSA-13)). *J. Surf. Anal*. 2014;20(3):155−160. https://doi.org/10.1384/jsa.20.155

85. Powell C.J., Jablonski A. Progress in quantitative surface analysis by X-ray photoelectron spectroscopy: current status and perspectives. *J. Electron Spectrosc.* 2010;178–179:331–346. https://doi.org/10.1016/j.elspec.2009.05.004

86. Powell C.J., Tougaard S., Werner W.S.M., Smekal W. Sample-morphology effects on X-ray photoelectron peak intensities. *J. Vac. Sci. Technol. A*. 2013;31(2):021402(7 p.). https://doi.org/10.1116/1.4774214

87. Powell C.J., Werner W.S.M., Smekal W. Sample-morphology effects on X-ray photoelectron peak intensities. II. Estimation of detection limits for thin-film materials. *J. Vac. Sci. Technol.* A. 2014;32(5):050603(6 p.). https://doi.org/10.1116/1.4891628

88. Leckey R. Ultraviolet Photoelectron Spectroscopy of Solids. In: O'Connor D.J., Sexton B.A., Smart R.S.C. (Eds.). *Surface Analysis Methods in Materials Science. Springer Series in Surface Sciences*. Berlin Heidelberg: Springer; 1993. V. 23. P. 291–300. https://doi.org/10.1007/978-3-662-02767-7_14

89. Doh W. H., Papaefthimiou V., Dintzer T., Dupuis V., Zafeiratos S. Synchrotron Radiation X-ray Photoelectron Spectroscopy as a Tool to Resolve the Dimensions of Spherical Core/Shell Nanoparticles. *J. Phys. Chem. C.* 2014;118(46):26621−26628. https://doi.org/10.1021/jp508895u

90. Fitch A.N. 2.10 – Synchrotron Methods. In: Constable E.C., Parkin G., Que Jr.L. (Eds.). *Comprehensive Coordination Chemistry III*. Elsevier; 2021. P. 160–182. ISBN 9780081026892. https://doi.org/10.1016/B978-0-12-409547-2.14660-8

91. Nemšák S., Shavorskiy A., Karslioglu O., Zegkinoglou I., Rattanachata A., Conlon C.S., Keqi A., Greene P.K., Burks E.C., Salmassi F., Gullikson E.M., Yang S.-H., Liu K., Bluhm H., Fadley C.S. Concentration and chemical-state profiles at heterogeneous interfaces with sub-nm accuracy from standing-wave ambient-pressure photoemission. *Nat. Commun*. 2014;5:5441–5447. https://doi.org/10.1038/ncomms6441

92. Fetisov G.V. X-ray diffraction methods for structural diagnostics of materials: progress and achievements. *Phys.-Usp*. 2020;63(1)2–32. https://doi.org/10.3367/UFNe.2018.10.038435

93. Karslioglu O., Nemsak S., Zegkinoglou I., Shavorskiy A., Hartl M., Salmassi F., Gullikson E.M., Ng M.L., Rameshan Ch., Rude B., Bianculli D., Cordones A.A., Axnanda S., Crumlin E.J., Ross P.N., Schneider C.M., Hussain Z., Liu Z., Fadley C.S., Bluhm H. Aqueous solution/metal interfaces investigated in operando by photoelectron spectroscopy. *Faraday Discuss.* 2015;180:35–53. https://doi.org/10.1039/c5fd00003c

94. Kjærvik M., Hermanns A., Dietrich P., Thissen A., Bahr S., Ritter B., Kemnitz E., Unger W.E.S. Detection of suspended nanoparticles with near-ambient pressure X-ray photoelectron spectroscopy. *J. Phys.: Condens. Matter.* 2017;29(47):474002(9 p.). https://doi.org/10.1088/1361-648x/aa8b9d

95. Corcoran C.J., Tavassol H., Rigsby M.A., Bagus P., Wieckowski A. Application of XPS to study electrocatalysts for fuel cells. *J. Power Sources*. 2010;195(24):7856–7879. https://doi.org/10.1016/j.jpowsour.2010.06.018

96. Brown M. A., Redondo A. B., Sterrer M., Winter B., Pacchioni G., Abbas Z., van Bokhoven J.A. Measure of Surface Potential at the Aqueous−Oxide Nanoparticle Interface by XPS from a Liquid Microjet. *Nano Lett*. 2013;13(11):5403−5407. https://doi.org/10.1021/nl402957y

97. Baer D.R., Engelhard M.H., Johnson J.E., Laskin J., Lai J., Mueller K., Munusamy P., Thevuthasan S., Wang H., Washton N. Surface characterization of nanomaterials and nanoparticles: important needs and challenging opportunities. *J. Vac. Sci. Technol. A*. 2013;31(5):050820–050854. https://doi.org/10.1116/1.4818423

98. Liu X., Zhang X., Bo V., Li L., Tian H., Nie Y., Sun Y., Xu S., Wang Y, Zheng W., Sun C.Q. Coordination-Resolved Electron Spectrometrics. *Chem. Rev*. 2015;115(14):6746–6810. https://doi.org/10.1021/cr500651m

99. Sublemontier O., Nicolas C., Aureau D., Patanen M., Kintz H., Liu X., Gaveau M.-A., Le Garrec J.-L., Robert E., Barreda F.-A., Etcheberry A., Reynaud C., Mitchell J.B., Miron C. X-ray Photoelectron Spectroscopy of Isolated Nanoparticles. *J. Phys. Chem. Lett*. 2014;5(19):3399−3403. https://doi.org/10.1021/jz501532c

100. Jiang Z.X., Alkemade P.F.A. The surface transient in Si for SIMS with oblique low-energy O_2^+ beams. *Surf. Interface Anal.* 1999;27(3):125–131. https://doi.org/10.1002/(SICI)1096-9918(199903)27:3<125::AID-SIA490>3.0.CO;2-8

101. Hajati S., Tougaard S. XPS for non-destructive depth profiling and 3D imaging of surface nanostructures. *Anal. Bioanal. Chem.* 2010;396(8):2741–2755. https://doi.org/10.1007/s00216-009-3401-9

102. Sostarecz A.G., McQuaw C.M., Wucher A., Winograd N. Depth Profiling of Langmuir-Blodgett Films with a Buckminsterfullerene Probe. *Anal. Chem*. 2004;76(22):6651–6658. https://doi.org/10.1021/ac0492665

103. Kozole J., Szakal C., Kurczy M., Winograd N. Model multilayer structures for three-dimensional cell imaging. *Appl. Surf. Sci*. 2006;252(19):6789–6792. https://doi.org/10.1016/j.apsusc.2006.02.209

104. Conlan X.A., Gilmore I.S., Henderson A., Lockyer N., Vickerman J. Polyethylene terephthalate (PET) bulk film analysis using C_{60}^+, Au_3^+, and Au^+ primary ion beams. *Appl. Surf. Sci.* 2006;252(19):6562–6565. https://doi.org/10.1016/j.apsusc.2006.02.068

105. Sakai Y., Iijima Y., Takaishi R., Asakawa D., Hiraoka K. Depth Profiling of Polystyrene Using Charged Water Droplet Impact. *J. Surf. Anal*. 2009;15(3):283–286. https://doi.org/10.1384/jsa.15.283

106. Galindo R.E., Gago R., Albella J., Lousa A. Comparative depth-profiling analysis of nanometer-metal multilayers by ion-probing techniques. *TrAC Trends Anal. Chem*. 2009;28(4):494–505. https://doi.org/10.1016/j.trac.2009.01.004

107. Bakaleinikov L.A., Domracheva Ya.V., Zamoryanskaya M.V., Kolesnikova E.V., Popova T.B., Flegontova E.Yu. Depth profiling of semiconductor structures by X-ray microanalysis using the electron probe energy variation technique. *Semiconductors*. 2009;43(4):544–549. https://doi.org/10.1134/S1063782609040265

[Original Russian Text: Bakaleinikov L.A., Domracheva Ya.V., Zamoryanskaya M.V., Kolesnikova E.V., Popova T.B., Flegontova E.Yu. Depth profiling of semiconductor structures by X-ray microanalysis using the electron probe energy variation technique. *Fizika i Tekhnika Poluprovodnikov*. 2009;43(4):568–576 (in Russ.).]

108. Jablonski A., Powell C.J. Practical expressions for the mean escape depth, the information depth, and the effective attenuation length in Auger-electron spectroscopy and X-ray photoelectron spectroscopy. *J. Vac. Sci. Technol. A.* 2009;27(2):253–261. https://doi.org/10.1116/1.3071947

109. Hesse R., Weiß M., Szargan R., Streubel P., Denecke R. Comparative study of the modelling of the spectral background of photoelectron spectra with the Shirley and improved Tougaard methods. *J. Electron. Spectros. Relat. Phenomena*. 2013;186:44–53. https://doi.org/10.1016/j.elspec.2013.01.020

110. Tougaard S. Practical guide to the use of backgrounds in quantitative XPS. *J. Vac. Sci. Technol. A.* 2021;39(1):011201(22 p.). https://doi.org/10.1116/6.0000661

111. Engelhard M.H., Baer D.R., Herrera-Gomez A., Sherwood P. Introductory guide to backgrounds in XPS spectra and their impact on determining peak intensities. *J. Vac. Sci. Technol. A*. 2020;38(6):063203(24 p.). https://doi.org/10.1116/6.0000359

112. Jain V., Biesinger M.C., Linford M.R. The Gaussian-Lorentzian Sum, Product, and Convolution (Voigt) functions in the context of peak fitting X-ray photoelectron spectroscopy (XPS) narrow scans. *Appl. Surf. Sci.* 2018;447:548–553. https://doi.org/10.1016/j.apsusc.2018.03.190

113. Hesse R., Weiß M., Szargan R., Streubel P., Denecke R. Improved peak-fit procedure for XPS measurements of inhomogeneous samples—Development of the advanced Tougaard background method. *J. Electron Spectros. Relat. Phenomena*. 2015;205:29–51. https://doi.org/10.1016/j.elspec.2015.06.013

114. Zborowski C., Vanleenhove A., Conard T. Comparison and complementarity of QUASES-Tougaard and SESSA software. *Appl. Sur. Sci*. 2022;585:152758(8 p.). https://doi.org/10.1016/j.apsusc.2022.152758

115. Briggs D., Seah P. (Eds.). *Practical surface analysis: Auger and X-ray photoelectron spectroscopy*. Chichester: John Wiley & Sons; 1996. V. 1. 674 p.

116. Sun C.Q. Size dependence of nanostructures: Impact of bond order deficiency. *Prog. Solid State Ch.* 2007;35(1):1–159. https://doi.org/10.1016/j.progsolidstchem.2006.03.001

117. Hill J., Royce D.G., Fadley C.S., Wagner L.F., Grunthaner F.J. Properties of oxidized silicon as determined by angular-dependent X-ray photoelectron spectroscopy. *Chem. Phys. Lett.* 1976;44(2):225–231. https://doi.org/10.1016/0009-2614(76)80496-4

118. Seah M.P. Intercomparison of silicon dioxide thickness measurements made by multiple techniques: The route to accuracy. *J. Vac. Sci. Technol. A*. 2004;22(4):1564–1571. https://doi.org/10.1116/1.1705594

119. Tougaard S. Energy loss in XPS: Fundamental processes and applications for quantification, non-destructive depth profiling and 3D imaging. *J. Electron. Spectrosc. Relat. Phenom*. 2010;178–179:128–153. https://doi.org/10.1016/j.elspec.2009.08.005

120. Tougaard S. Universality Classes of Inelastic Electron Scattering Cross-sections. *Surf. Interface Anal.* 1997;25(3):137–154. https://doi.org/10.1002/(SICI)1096-9918(199703)25:3<137::AID-SIA230>3.0.CO;2-L

121. Tougaard S. Quantification of Nanostructures by Electron Spectroscopy. In: Briggs D., Grant J.T. (Eds.). *Surface Analysis by Auger and X-Ray Photoelectron Spectroscopy*. IM Publications; 2003. P. 295–343.

122. Iwai H., Hammond J.S., Tanuma S. Recent status of thin film analyses by XPS. *J. Surf. Anal*. 2009;15(3):264–270. https://doi.org/10.1384/jsa.15.264

123. Gunter P.L.J., Dejong A.M., Niemantsverdriet J.W., Rheiter H.J.H. Evaluation of take-off angle-dependent XPS for determining the thickness of passivation layers on aluminum and silicon. *Surf. Interface Anal*. 1992;19(1–12):161–164. https://doi.org/10.1002/sia.740190131

124. Cole D.A., Shallenberger J.R., Novak S.W., Moore R.L. SiO_2 thickness determination by X-ray photoelectron spectroscopy, Auger electron spectroscopy, secondary ion mass spectrometry, Rutherford backscattering, transmission electron microscopy, and ellipsometry. *J. Vac. Sci. Technol. B.* 2000;18(1):440–444. https://doi.org/10.1116/1.591208

125. Alexander M.R., Thompson G.E., Zhou X., Beamson G., Fairley N. Quantification of oxide film thickness at the surface of aluminum using XPS. *Surf. Interface Anal.* 2002;34(1):485–489. https://doi.org/10.1002/sia.1344

126. Olsson C.-O.A., Landolt D. Atmospheric oxidation of a Nb-Zr alloy studied with XPS. *Corros. Sci.* 2004;46(1):213–224. https://doi.org/10.1016/S0010-938X(03)00139-2

127. Kappen P., Reihs K., Seidel C., Voetz M., Fuchs H. Overlayer thickness determination by angular dependent X-ray photoelectron spectroscopy (ADXPS) of rough surfaces with a spherical topography. *Surf. Sci.* 2000;465(1–2):40–50. https://doi.org/10.1016/S0039-6028(00)00653-1

128. Martin-Concepcion A.I., Yubero F., Espinos J.P., Tougaard S. Surface roughness and island formation effects in ARXPS quantification. *Surf. Interface Anal.* 2004;36(8):788–792. https://doi.org/10.1002/sia.1765

129. Cumpson P.J. Thickogram: A method for easy film thickness measurement in XPS. *Surf. Interface Anal*. 2000;29(6):403–406. https://doi.org/10.1002/1096-9918(200006)29:6<403::AID-SIA884>3.0.CO;2-8

130. Cui Yi-T., Tougaard S., Oji H., Son J.-Y., Sakamoto Y., Matsumoto T., Yang A., Sakata O., Song H., Hirosawa I. Thickness and structure of thin films determined by background analysis in hard X-ray photoelectron spectroscopy. *J. Appl. Phys*. 2017;121(22):225307-1-10. https://doi.org/10.1063/1.4985176

131. Tougaard S. Novel Applications of Inelastic Background XPS Analysis: 3D Imaging and HAXPES. *J. Surf. Anal.* 2017;24(2):107–114. https://doi.org/10.1384/jsa.24.107

132. Paynter R.W. An ARXPS primer. *J. Electron. Spectrosc. Relat. Phenom*. 2009;169(1):1–9. https://doi.org/10.1016/j.elspec.2008.09.005

133. Cumpson P.J. Angle-resolved XPS and AES: depth-resolution limits and a general comparison of properties of depth-profile reconstruction methods. *J. Electron. Spectrosc. Relat. Phenom*. 1995;73(1):25–52. https://doi.org/10.1016/0368-2048(94)02270-4

134. Oswald S., Oswald F. Computer simulation of angle-resolved X-ray photoelectron spectroscopy measurements for the study of surface and interface roughnesses. *J. Appl. Phys*. 2006;100(10):104504(9 p.). https://doi.org/10.1063/1.2386938

135. Oswald S., Oswald F. A promising concept for using near-surface measuring angles in angle-resolved X-ray photoelectron spectroscopy considering elastic scattering effects. *J. Appl. Phys*. 2011;109(3):034305(11 p.). https://doi.org/10.1063/1.3544002

136. Herrera-Gomez A., Grant J. T., Cumpson P., Jenko M., Aguirre-Tostado F.S., Brundle C.R., Conard T., Conti G., Fadley C.S., Fulghum J., Kobayashi K., Kövér L., Nohira H., Opila R.L., Oswald S., Paynter R.W., Wallace R.M., Werner W.S.M., Wolstenholme J. Report on the 47th IUVSTA Workshop "Angle-Resolved XPS: The current status and future prospects for angle-resolved XPS of nano and subnano films." *Surf. Interface Anal.* 2009;41(11):840–857. https://doi.org/10.1002/sia.3105

137. Liu Y., Hofmann S., Wang J.Y. An analytical depth resolution function for the MRI model. *Surf. Interface Anal.* 2013;45(11–12):1659–1660. https://doi.org/10.1002/sia.5319

138. Yang J., Li W., Wang D., Li Y. Electronic Metal–Support Interaction of Single-Atom Catalysts and Applications in Electrocatalysis. *Adv. Mater.* 2020;32(49):2003300(29 p.). https://doi.org/10.1002/adma.202003300

139. Moretti G. Auger parameter and Wagner plot in the characterization of chemical states by X-ray photoelectron spectroscopy: a review. *J. Electron. Spectrosc. Relat. Phenom.* 1998;95(2–3):95–144. https://doi.org/10.1016/S0368-2048(98)00249-7

140. Moretti G. The Wagner plot and the Auger parameter as tools to separate initial- and final-state contributions in X-ray photoemission spectroscopy. *Surf. Sci.* 2013;618:3–11. https://doi.org/10.1016/j.susc.2013.09.009

141. Zafeiratos S., Kennou A.A study of gold ultrathin film growth on yttria-stabilized ZrO_2(100). *Surf. Sci.* 1999;443(3):238–244. https://doi.org/10.1016/S0039-6028(99)01014-6

142. Fu Q., Wagner T. Interaction of nanostructured metal overlayers with oxide surfaces. *Surf. Sci. Rep.* 2007;62(11):431–498. https://doi.org/10.1016/j.surfrep.2007.07.001

143. Fulghum J.E., Linton R.W. Quantitation of coverages on rough surfaces by XPS: an overview. *Surf. Interface Anal.* 1988;13(4):186–192. https://doi.org/10.1002/sia.740130404

144. Werner W.S.M., Chudzicki M., Smekal W., Powell C. Interpretation of nanoparticle X-ray photoelectron intensities. *Appl. Phys. Lett*. 2014;104(24):243106(3 p.). https://doi.org/10.1063/1.4884065

145. Frydman A., Castner D.G., Schmal M., Campbell C. A method for accurate quantitative XPS analysis of multimetallic or multiphase catalysts on support particles. *J. Catal.* 1995;157(1):133–144. https://doi.org/10.1006/jcat.1995.1274

146. Martin J.E., Herzing A.A., Yan W., Li X.-Q., Koel B.E., Kiely C.J., Zhang W.-X. Determination of the oxide layer thickness in core-shell zerovalent iron nanoparticles. *Langmuir.* 2008;24(8):4329–4334. https://doi.org/10.1021/la703689k

147. Tunc I., Suzer S., Correa-Duarte M.A., Liz-Marzan L. XPS Characterization of Au(Core)/SiO_2 (Shell) Nanoparticles. *J. Phys. Chem*. B. 2005;109(16):7597–7600. https://doi.org/10.1021/jp050767j

148. Diebold U., Pan J.-M., Madey T.E. Growth mode of ultrathin copper overlayers on TiO_2(110). *Phys. Rev. B.* 1993;47(7):3868–3876. https://doi.org/10.1103/PhysRevB.47.3868

149. Sharp J.C., Campbell C.T. Quantitative modeling of electron spectroscopy intensities for supported nanoparticles: The hemispherical cap model for non-normal detection. *Surf. Sci.* 2015;632:L5–L8. https://doi.org/10.1016/j.susc.2014.08.010

150. Yang D.Q., Gillet J.N., Meunier M., Sacher E. Room temperature oxidation kinetics of Si nanoparticles in air, determined by X-ray photoelectron spectroscopy. *J. Appl. Phys.* 2005;97(2):24303(6 p.). https://doi.org/10.1063/1.1835566

151. Vazquez-Pufleau M.A. Simple Model for the High Temperature Oxidation Kinetics of Silicon Nanoparticle Aggregates. *Silicon.* 2021;13(3):189–200. https://doi.org/10.1007/s12633-020-00415-3

152. Gillet J.N., Meunier M. General equation for size nanocharacterization of the core-shell nanoparticles by X-ray photoelectron spectroscopy. *J. Phys. Chem. B.* 2005;109(18):8733–8737. https://doi.org/10.1021/jp044322r

153. Shard A.G., Wang J., Spencer S.J. XPS Topofactors: Determining Overlayer Thickness on Particles and Fibres. *Surf. Interface Anal.* 2009;41(7):541–548. https://doi.org/10.1002/sia.3044

154. Patrone L., Nelson D., Safarov V.I., Sentis M., Marine W. Photoluminescence of silicon nanoclusters with reduced size dispersion produced by laser ablation. *J. Appl. Phys.* 2000;87(8):3829–3837. https://doi.org/10.1063/1.372421

155. Hofmeister H., Huisken F., Kohn B. Lattice contraction in nanosized silicon particles produced by laser pyrolysis of silane. *Eur. Phys. J. D.* 1999;9(1–4):137–140. https://doi.org/10.1007/s100530050413

156. Werner W.S.M., Smekal W., Powell C.J. *Simulation of Electron Spectra for Surface Analysis. Version 2.1 User's Guide.* 2017. 134 p. https://doi.org/10.6028/NIST.NSRDS.100-2017. Accessed April 01, 2023.

157. Risterucci P., Renault O., Zborowski C., Bertrand D., Torres A., Rueff J.-P., Ceolin D.,Grenet G., Tougaard S. Effective inelastic scattering cross-sections for background analysis in HAXPES of deeply buried layers. *Appl. Surf. Sci*. 2017;402:78–85. https://doi.org/10.1016/j.apsusc.2017.01.046

158. Baer D.R., Wang Y.-C., Castner D.J. Use of XPS to Quantify Thickness of Coatings on Nanoparticles. *Micros. Today*. 2016;24(2):40–45. https://doi.org/10.1017/S1551929516000109

159. Pauly N., Tougaard S., Yubero F. Modeling of X-ray photoelectron spectra: surface and core hole effects. *Surf. Interface Anal*. 2014;46(10–11):920–923. https://doi.org/10.1002/sia.5372

160. Hajati S., Zaporojtchenko V., Faupel F., Tougaard S. Characterization of Au nano-cluster formation on and diffusion in polystyrene using XPS peak shape analysis. *Surf. Sci*. 2007;601(15):3261–3267. https://doi.org/10.1016/j.susc.2007.06.001

161. Mansilla C., Gracia F., Martin-Concepcion A.I., Espinós J.P., Holgado J.P., Yubero F., González-Elipe A.R. Study of the first nucleation steps of thin films by XPS inelastic peak shape analysis. *Surf. Interface Anal.* 2007;39(4):331–336. https://doi.org/10.1002/sia.2509

162. Mourdikoudis S., Pallares R.M., Thanh N.T.K. Characterization techniques for nanoparticles: comparison and complementarity upon studying nanoparticle properties. *Nanoscale*. 2018;10(27):12871–12934. https://doi.org/10.1039/C8NR02278J

163. Baer D.R. Guide to making XPS measurements on nanoparticles. *J. Vac. Sci. Technol. A.* 2020;38(3):031201. https://doi.org/10.1116/1.5141419

164. Baer D.R., Wang Y.-C., Castner D.J. Use of XPS to Quantify Thickness of Coatings on Nanoparticles. *Micros. Today*. 2016;24(2):40–45. https://doi.org/10.1017/S1551929516000109

165. Kjærvik M., Hermanns A., Dietrich P., Thissen A., Bahr S., Ritter B., Kemnitz E., Unger W.E.S. Detection of suspended nanoparticles with near-ambient pressure X-ray photoelectron spectroscopy. *J. Phys.: Condens. Matter.* 2017;29(47):474002(9 p.). https://doi.org/10.1088/1361-648x/aa8b9d

About the authors:

Anatoly A. Ischenko, Dr. Sci. (Chem.), Professor, Head of the I.P. Alimarin Department of Analytical Chemistry, M.V. Lomonosov Institute of Fine Chemical Technologies, MIREA – Russian Technological University (86, Vernadskogo pr., Moscow, 119571, Russia). E-mail: aischenko@yasenevo.ru. Scopus Author ID 6701507307, ResearcherID B-2767-2014, https://orcid.org/0000-0003-1532-377X

Mikhail A. Lazov, Cand. Sci. (Chem.), Assistant Professor, I.P. Alimarin Department of Analytical Chemistry, M.V. Lomonosov Institute of Fine Chemical Technologies, MIREA – Russian Technological University (86, Vernadskogo pr., Moscow, 119571, Russia). E-mail: lazovm@gmail.com. Scopus Author ID 56466030700, https://orcid.org/0000-0001-8578-1683

Elena V. Mironova, Senior Lecturer, I.P. Alimarin Department of Analytical Chemistry, M.V. Lomonosov Institute of Fine Chemical Technologies, MIREA – Russian Technological University (86, Vernadskogo pr., Moscow, 119571, Russia). E-mail: mironova.ev.mitht@yandex.ru. https://orcid.org/0000-0001-8213-7059

Alexey Yu. Putin, Cand. Sci. (Chem.), Assistant Professor, Department of General Chemical Technology, M.V. Lomonosov Institute of Fine Chemical Technologies, MIREA – Russian Technological University (86, Vernadskogo pr., Moscow, 119571, Russia). E-mail: putin@mirea.ru. https://orcid.org/0000-0003-1333-7318

Andrey M. Ionov, Dr. Sci. (Phys.-Math.), Professor, Leading Researcher, Osipyan Institute of Solid State Physics, Russian Academy of Sciences (2, Akademika Osip'yana ul., Chernogolovka, Moscow oblast, 142432, Russia). E-mail: ionov@issp.ac.ru. https://orcid.org/0000-0002-2094-1065

Pavel A. Storozhenko, Academician at the Russian Academy of Sciences, Dr. Sci. (Chem.), Professor, Scientific Director of State Scientific Research Institute of Chemistry and Technology of Organoelement Compounds (38, Entuziastov shosse, Moscow, 111123, Russia). E-mail: bigpastor@mail.ru. Scopus Author ID 9633186700, ResearcherID D-4645-214

Об авторах:

Ищенко Анатолий Александрович, д.х.н., профессор, заведующий кафедрой аналитической химии им. И.П. Алимарина Института тонких химических технологий им. М.В. Ломоносова ФГБОУ ВО «МИРЭА – Российский технологический университет» (119571, Россия, Москва, пр-т Вернадского, д. 86). E-mail: aischenko@yasenevo.ru. Scopus Author ID 6701507307, ResearcherID B-2767-2014, https://orcid.org/0000-0003-1532-377X

Лазов Михаил Александрович, к.х.н., ассистент кафедры аналитической химии им. И.П. Алимарина Института тонких химических технологий им. М.В. Ломоносова ФГБОУ ВО «МИРЭА – Российский технологический университет» (119571, Россия, Москва, пр-т Вернадского, д. 86). E-mail: lazovm@gmail.com. Scopus Author ID 56466030700, https://orcid.org/0000-0001-8578-1683

Миронова Елена Валерьевна, старший преподаватель кафедры аналитической химии им. И.П. Алимарина Института тонких химических технологий им. М.В. Ломоносова ФГБОУ ВО «МИРЭА – Российский технологический университет» (119571, Россия, Москва, пр-т Вернадского, д. 86). E-mail: mironova.ev.mitht@yandex.ru. https://orcid.org/0000-0001-8213-7059

Путин Алексей Юрьевич, к.х.н., доцент кафедры общей химической технологии Института тонких химических технологий им. М.В. Ломоносова ФГБОУ ВО «МИРЭА – Российский технологический университет» (119571, Россия, Москва, пр-т Вернадского, д. 86). E-mail: putin@mirea.ru. https://orcid.org/0000-0003-1333-7318

Ионов Андрей Михайлович, д.ф.-м.н., профессор, ведущий научный сотрудник, ФГБУН «Институт физики твердого тела им. Ю.А. Осипьяна» Российской академии наук (142432, Россия, Московская обл., г. Черноголовка, ул. Академика Осипьяна, д. 2). E-mail: ionov@issp.ac.ru. https://orcid.org/0000-0002-2094-1065

Стороженко Павел Аркадьевич, академик РАН, д.х.н., профессор, научный руководитель ГНЦ РФ АО «Государственный научно-исследовательский институт химии и технологии элементоорганических соединений» (111123, Россия, Москва, шоссе Энтузиастов, д. 38). E-mail: bigpastor@mail.ru. Scopus Author ID 9633186700, ResearcherID D-4645-214

The article was submitted: June 06, 2022; approved after reviewing: November 07, 2022; accepted for publication: March 27, 2023.

Translated from Russian into English by H. Moshkov